Bachelor thesis

Department of automotive and aeronautical engineering

A comparative study between winglet and raked wingtip wing configurations

Tom-Robin Teschner

16. Juli 2012

Hochschule für Angewandte Wissenschaften Hamburg
Fakultät Technik und Informatik
Department Fahrzeugtechnik + Flugzeugbau
Berliner Tor 9
20099 Hamburg

In cooperation with:

Universidad de Sevilla
Escuela Técnica Superior de Ingeniería
Camino de los Descubrimientos, s/n
Isla de la Cartuja
41092 Sevilla

Author: Tom-Robin Teschner
Due: 30.07.2012

1. Examiner: Prof. Hartmut Zingel
2. Examiner: Prof. Detlef Schulze

Supervisor: Prof. José Manuel Gordillo Arias de Saavedra

Table of content

1 Introduction

1.1 Abstract

The impact on the reduction in reduced drag for a raked wingtip and winglet configuration was investigated at the University of Seville and compared against a clean wing configuration with no wingtip attached. The results were obtained by experiments in the wind tunnel facilities as well as numerically using the software package FLUENT from ANSYS. To find the optimal winglet configuration several iterations with different designs were done while the raked wingtip does depend heavily on boundary conditions so no iterations had to be done. Both preliminary designs were created in the free vortex-lattice code TORNADO for MATLAB. The results were taken for a detailed design in CATIA V5. Those design were the basis for the numerical investigation but served also as the master geometry for the rapid prototyping. The models were directly printed at the University's 3D-printer which were later used for the wind tunnel experiments. To obtain the induced drag the classical Trefftz-plane analyze has been applied to the FLUENT results while the experimentally data had to be processed in a different way. Two alternative approaches are presented, one of which is too unstable to produce reliable results while the other approach works better given the right boundary conditions. It has been showed that the winglet reduces the induced drag the most while the raked wingtip reduces the induced drag as well but not as effective as the winglet. The raked wingtip might offer a weight reduction at the wing root due to its ability to reduce the bending and twisting moment as well but it was beyond the scope of the present investigation to give proof.

1.2. Acknowledgements

1.3. List of Symbols

Alphabetic symbols (capital)

C_B	Root bending moment coefficient	[ ]
C_L	Lift coefficient	[ ]
c_L	Local lift coefficient	[ ]
$C_L(\alpha)$	Slope of the lift coefficient	[1/rad]
C_{Di}	Induced drag coefficient	[ ]
C_p	Pressure coefficient	[ ]
D_i	Induced Drag	[N]
L	Lift	[N]
Ma	Mach number	[ ]
M_r	Root bending moment	[Nm]
P	Any arbitrary point in a flow field	[ ]
S	Surface area of wing	[m²]
S_T	Trefftz-plane	[m²]
U_∞	Free stream velocity	[m/s]
U	Velocity Vector	[m/s]
V_i	Induced velocity	[m/s]

Alphabetic symbols

b	Span of wing	[m]
c	Chord length	[m]
c_{MAC}	Mean aerodynamic chord	[m]
e	Oswald efficiency number	[ ]
e_0	Internal energy	[Nm]
e_a	Apparent error	[ ]
e_{ext}	Extrapolated error	[ ]
f	Force exerted on a body	[N]
g	Gravity	[m/s²]
h	Representative mesh size	[m]
l	Weight coefficient	[ ]
p	Pressure	[N/m²]
p_∞	Static pressure	[N/m²]
r	Ratio of fine to coarse mesh	[ ]
t	Time	[s]
$\dot{q}$	Heat change	[Nm/s]
u	x-velocity component	[m/s]
v	y-velocity component	[m/s]
w	z-velocity component	[m/s]

Greek symbols

Γ	Circulation	[m²/s]
Λ	aspect ratio	[ ]
ϕ	Flow property	[ ]
λ	Taper ratio	[ ]
μ	Viscosity	[kg/s m]
ρ	Density	[kg/m³]

Abbreviations

CFD	Computation fluid dynamics
FFT	Fast fourier transformation
FSI	Fluid-structure interaction
GCI	Grid convergence index

1.4 Statutory declaration

 I herewith declare that I have completed the present thesis independently making use only of the specified literature and aids. Sentences or parts of sentences quoted literally are marked as quotations; identification of other references with regard to the statement and scope of the work is quoted. The thesis in this form or in any other form has not been submitted to an examination body and has not been published.

Date:_____   Signature:_____

2.   About wingtip devices

2.1.   A brief history on the development of wingtip devices

In 1897, six years before the first successful powered flight, Frederick William Lanchester was the first person to notice that wingtip modification under certain circumstances would lead to a reduction in wingtip vortices. Lanchester, who laid the groundwork for Prandtl's lifting line theory, was rejected with his work, being too advanced for his time. In 1910, William E. Somerville received a patent for his curled up wing who was as well the first one to fly an airplane with wingtip modifications. Later in 1930, Vincent Burnelli received US patent number 1,775,474 for his "end plating wing tips". Sighard Hoerner invented a new wingtip modification in 1952 that pushes the vortex further outward, thus increasing the effective span and thereby reducing the induced drag. This design can still be found on small aircrafts nowadays.

Aircraft technology increased rapidly but the effects of wingtip modification played only a minor role in the design and research process. It was not until 1973 – the year of the oil crisis – that the interested in further drag reduction was raised. The aeronautical engineer Burt Rutan, known for his unusual-looking aircraft designs and his company TSC (The Spaceship Company) that was part of building Space Ship One, developed the first aircraft that used winglets as we know them today. The Rutan VariEze with winglets made its maiden flight on the 21st of May in 1975. One year later, the inventor of the area rule Richard T. Whitcomb investigated a winglet configuration at the NASA Langley research center [1]. He did that for a typical jet transport aircraft for that time at high subsonic speed. At the national business aviation association convention in 1977, the Learjet 28 was the first business aircraft to have winglets mounted at the end of their wings. It was planned to serve solely as an experimental prototype, however it outperformed its expectations so well that it resulted in a serial production.

The aviation industry started to developed an interest for wingtip devices and competitors around the world started to undertake research for various wingtip configurations. Boeing announced the predecessor of the Boeing 747-300 in 1985. Having the same aerodynamically shape, it was able to prolong its range by as much as 3.5% only due to the effect of added winglets. In the same year Airbus announced their predecessor of its Airbus 310-200, one of the improvements being added wingtip fences. Three years later the A320-200, fitted with the latest wingtip fences, was delivered to its first costumer. In 1993 and 1994, the Airbus A340 and A330 entered into service with a new design that differed from that seen before on any Airbus. Meanwhile, Boeing tried different forms and shapes of wingtip devices and came up with a complete new design, the so called raked wingtips. Rather than canting the wingtip up, thereby increasing the root bending moment, raked wingtips are an increase in span with a higher sweep angle and taper ratio thus yielding less induced drag and wingtip vortices by even less bending and twisting moment due to its special shape compared to winglets. They received a US patent in 1991 [2] and another in 2000 [3] which implied further improvements. In 2000, the Boeing 767-400ER entered into service with the new raked wingtip technology. In 2006 the Boeing 777-200LR followed that trend.
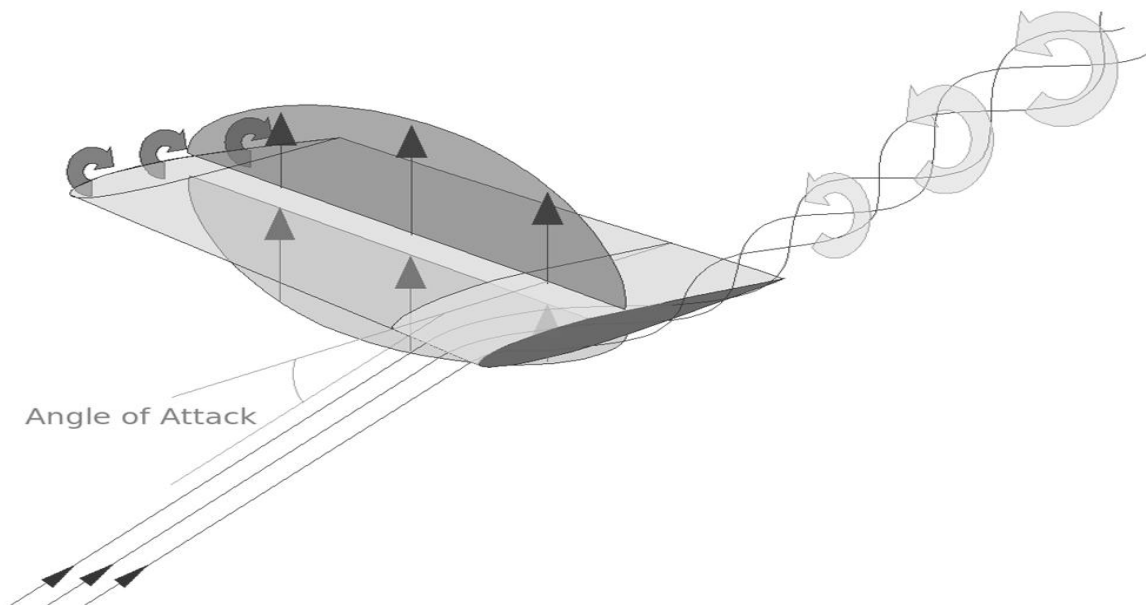
Figure 1

Boeing offered a retrofit winglet to its Boeing 737 classic and next-generation aircrafts in 2003, cutting down fuel cost by 4 to 6 percent. The winglet itself was called a blended winglet which allowed a further reduction in drag and less aerodynamical interference due to a blended transition between the junction of wing and winglet [4]. In 2009, Airbus introduced their new winglets for the A320 family (with exception to the A318) which they call sharklets. They are a new option for the A320 and the standard for the A320neo.

Ever since Whitcomb published his results there has been done a lot of research on wingtip devices. Mark D. Maughmer has made himself known in the aviation world for his contribution to winglets on sailplanes [5-7]. In a try and error process he designed the PSU-90-125 airfoil, specially made for sailplane winglets. The Idea of winglets for sailplanes was by no means new, however Maughmer was the first person who could successfully provided a winglet design that both increased the glide ratio and kept the parasite drag at a minimum level.

Today we are dealing with a great mixture between different forms of wingtip devices. The new Boeing 787 and Airbus 350 will have special wings, which do not have a separate winglet, but have raked, and blended wingtips integrated - without a sharp angle between the wing and the winglet.

Recent developments show that there is a blending process going on between different types of wingtip devices. Up until now there is no literature available for the public on the new designs and their effectiveness. Whether they are as useful or better as the current wingtip devices is still to be proven.

2.2.   Mode of operation of winglets and raked wingtips

Lift is generated because there is a lower pressure on the upper wing surface and a higher pressure on the lower wing surface. This effect will cause the flow to pass from the low pressure zone to the high pressure zone at the wingtip as can be seen in Figure 1. This crossflow at the wingtip generates
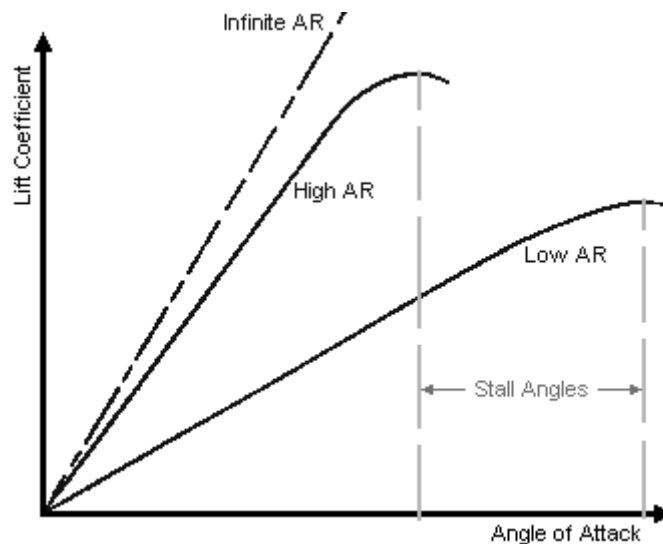
Figure 2

a vortex. The energy in the vortex originates from the flow around the wing hence the lost energy reduces the overall lift capability of the wing. This lost energy is referred to as induced drag which is defined as:

$$C_{D,i} = \frac{C_L^2}{\pi \Lambda e} \qquad (2.1)$$

The induced drag corresponds directly to the lift coefficient and the aspect ratio, which in turn is defined as:

$$\Lambda = \frac{b^2}{S} \qquad (2.2)$$

For a two dimensional case there is no crossflow which yields a higher slope for the lift coefficient, compared to a three dimensional case. This can be seen in Figure 2 for different aspect ratios. The higher the aspect ratio, the higher is the slope of C_L. A two dimensional case is defined for $\Lambda = \infty$ and it can be approximated by a very large span. Some typical values for different types of aircraft can be taken from Table 1.

Type of aircraft	Typical aspect ratio
Fighter jets	2 - 3
Small aircrafts	6 - 8
Business jets	7 - 8
Large commercial aircrafts	8 - 10
Sailplanes	20 - 50

Table 1
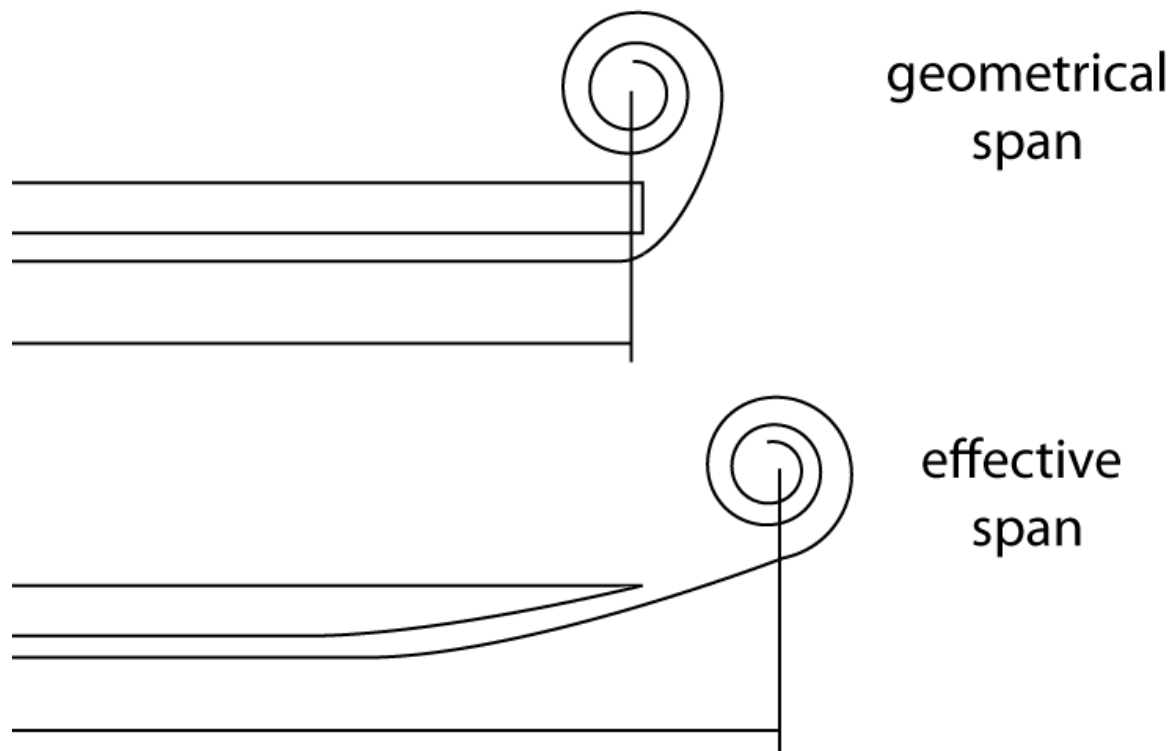
As can be seen, it is very important for sailplanes to reduce drag as much as possible hence the large value for the aspect ratio. This also corresponds directly to a very low roll rate for turns which would undermine the performance of fighter jets which therefore have a very low aspect ratio. All the other types of aircraft are located roughly in the same region. To reduce the induced drag it is logical that an increase of wingspan would do just that but it is not advisable or even possible in every case to do that. An increase in span automatically increases the root bending moment which in turn needs more structural mass. There are better ways to modify the wingtip to reduce the induced drag by keeping the bending moment at a minimum level that will be addressed in this chapter. But there is another fact that has to be considered. Since 2007, we have entered a new era of flight with the new Airbus A380. Up until then, the Boeing B747-400 was the world largest airplane (used for passenger transport) having a wingspan of 64.4 meters. The Airbus A380 topped it by having a massive 79.75 meters in span. Every aircraft is required to have less than 80 meters in span in order to be handled on ground at airports. Airports are designed to have no more than 80 meters space between each aircraft so that there is no space for an increase in span for the A380.

These, the increase in root bending moment due to a wing augmentation and the 80 meter airport space, are only two restrictions but there are several more which will not be addressed further since the present work is concerned about the aerodynamic performance.

In order to understand the mode of operation of winglets and raked wingtips it is mandatory to introduce a new definition for the span. So far, by talking about the span it was always the geometrical span that was meant. For just one wing, the span is measured from the wing root to the wingtip. The new span is called the effective span. It is measured from the wing root to the center of the vortex. It becomes more clearly by evaluating Figure 3. The upper sketch shows a rectangular

NET THRUST
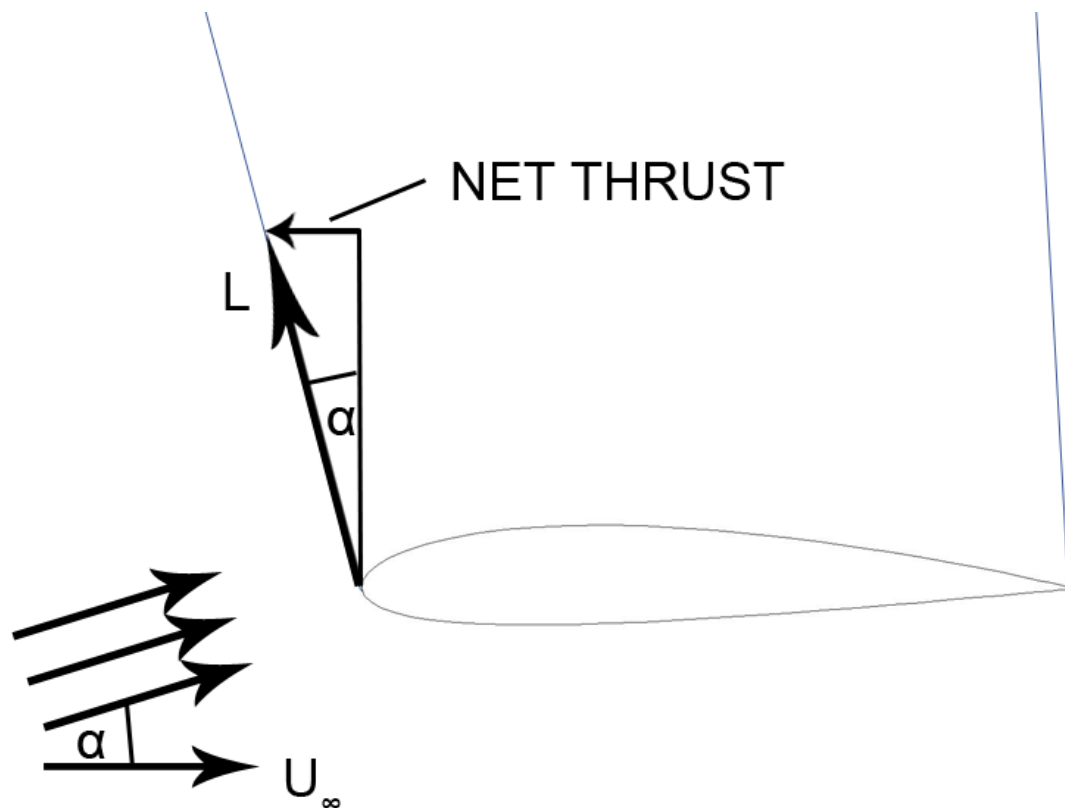
Figure 4

wing with no wingtip modification seen from behind. The air is flowing from the lower to the upper surface creating a vortex. This vortex has a center which in this case is just above the wingtip. On the lower sketch, the hoerner wingtip design can be seen. It just uses a rounded bottom surface. This design accelerates the flow in the direction lateral to the free stream pushing the flow further outwards resulting in a vortex further away from the wingtip. So on the upper sketch, the geometrical and effective span are the same while this is not true for the hoerner wingtip design on the lower sketch. What it does is basically increasing the effective span, therefore reducing the induced drag without increasing the geometrical span. Since the induced drag is due to the vortex it is only logical that the span form one vortex to the other should be used rather than the geometrical span.

Since 1976, when Richard T. Whitcomb published his results about his work on winglets there has been a booming on winglet research and they started to become more and more popular as well as a normal sight on aircrafts. Winglets reduce the vortices due to two reasons. The first one being that they are being canted upward, thereby increasing the span. In this case, the effective span is the geometrical span from the wing plus the height of the winglet [8]. The upward canted winglet has a fence like effect which makes it harder for the flow to cross from the lower to the upper surface. This also increases the lift coefficient so the reduction in vortices has to outplay this effect in order reduce the induced drag. The second reason is slightly less obvious but becomes more obvious when examining Figure 4. Due to the fact that there is a crossflow underneath the wing, this flow superimposed with the free stream will result in an inward pointed flow at the winglet. Now the lift vector can be split into their components normal and parallel to the free stream. There is a small vector pointing in the opposite direction of the free stream. This is referred to as net thrust [9] or,

Vortex filament
of strength Γ

dl

r

P

dV
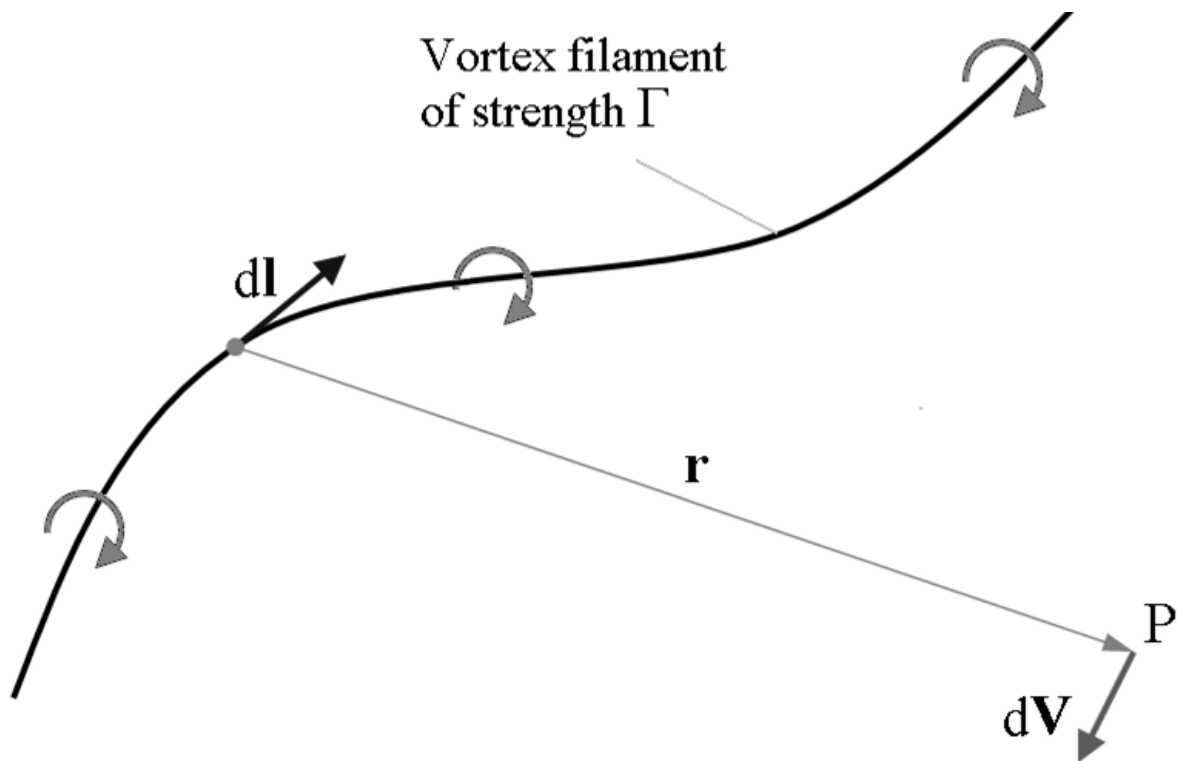
Figure 5

following the definition of drag and lift, it can be seen as negative drag. In order to achieve a high amount of net thrust, a high cambered airfoil should be used. Whitcomb referred to reference [10] to be a good starting point for the airfoil selection for the winglet design.

As mentioned before, the vortices get their energy from the crossflow. Now there is a small amount of that crossflow acting on the winglet which produces thrust, energy which otherwise would have been lost and used for creating a bigger vortex.

Raked wingtips on the other side use a different approach to cut down the vortices. They have a high sweep angle and a high taper ratio. The high taper ratio reduces the generation of vortices at the tip while the high sweep angle improves low speed characteristics during take-off and landing so it has not to be fitted with slats [3]. The center of pressure travels further back due to the high sweep angle. The lift produced on the raked wingtip generates a twisting moment that is now acting against the twisting moment generated by the main wing thereby reducing the overall twisting moment. New developments show raked wingtips that are curled upwards to push the crossflow further outwards. In this way, the vortices will be generated further outwards and thereby increasing the effective span which in turn will reduce the induced drag even more.

3.   Preliminary Sizing

3.1.   The Vortex-Lattice Method

Nowadays, with computer resources available at low costs, it has become very easy to investigate several configurations for any arbitrary aerodynamic shape. One of the most convenient ways is to

a)   b)   c)
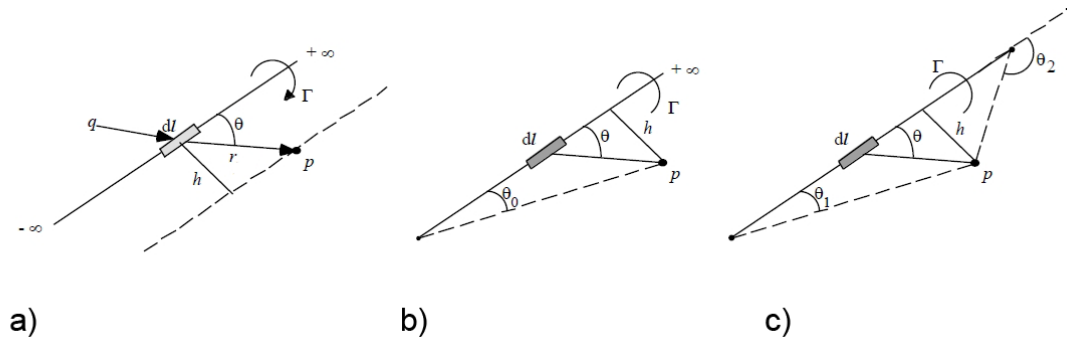
<div align="right">Figure 6</div>

use the Vortex-Lattice Method. The general concept is an expansion of the fundamental aerodynamic Biot-Savart law. This is sketched in Figure 5. The relating equation is:

$$dV_i = \frac{\Gamma}{4\pi} \frac{dl \times r}{|r|^3}$$
(3.1)

Here, dl is an infinite small section on the filament, r is the radius from point P to any point on the filament, Γ is the strength of the vortex and it is constant at every location. The Biot-Savart law is the relation between the induced velocity at any arbitrary point P due to the vortex filament. Equation (3.1) is given in its differential form. In order to obtain a value for the induced velocity it has to be integrated over the length of the vortex filament. Since the circulation has a constant value along the filament it can be taken out of the integration:

$$V_i = \frac{\Gamma}{4\pi} \int \frac{dl \times r}{|r|^3}$$
(3.2)

There are three different solutions for equation (3.2) each of them can be seen in Figure 6 with the corresponding nomenclature. Their integrated solutions are:

- a) For an infinite length of the vortex filament:

$$V_i = \frac{\Gamma}{2\pi h}$$
(3.3)

- b) For a semi-infinite length of the vortex filament:

$$V_i = \frac{\Gamma}{4\pi h}$$
(3.4)

- c) For a finite length of the vortex filament:

$$V_i = \frac{\Gamma}{4\pi h}(\cos\theta_1 - \cos\theta_2)$$
(3.5)
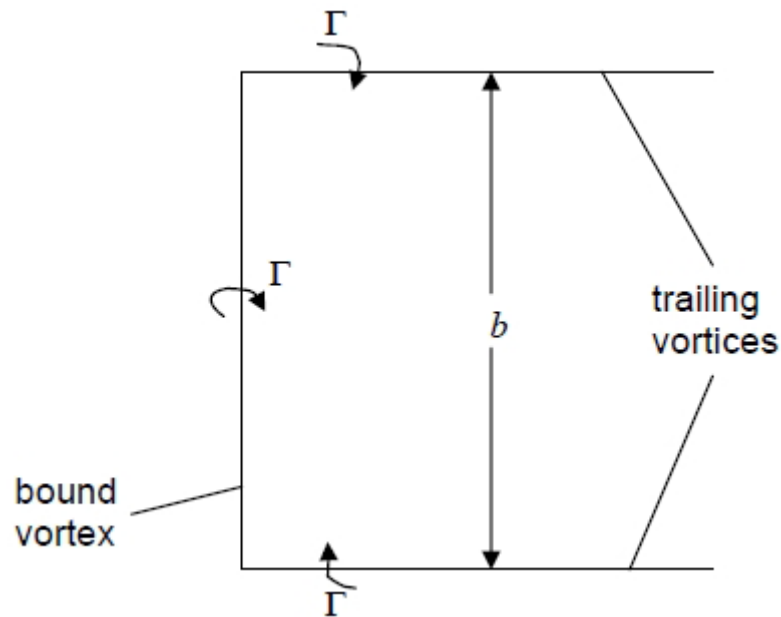
Figure 7

Here, h is the perpendicular distance from the vortex filament to point P and θ is the angle between the closing point and the point P with respect to h.

Ludwig Prandtl used this concept to create his lifting-line theory and replaced a straight rectangular wing by a horseshoe vortex as seen in Figure 7, consisting of two free-trailing vortices and one bounded vortex. This simple model is restricted to high aspect ratio wings. Furthermore it does not account for any geometrical deviation such as the sweep, twist or dihedral angle but for the relative simple case of a rectangular wing it yields accurate results. By obtaining the value of the circulation it is possible to calculate the lift. However it is obvious that this model has too many restrictions in order to be used for designing processes. The idea of the Vortex-Lattice Method is now to divide a wing of any arbitrary shape into small sections, the so called panels, to overcome this restriction. Each panel is equipped with its own horseshoe vortex, where the strength of the circulation and eventually the lift is calculated. That makes it possible to investigate more complex geometries. It was not before 1971 that a first, usable program was developed due to the limitation of computers at that time. Again, NASA was one of the first research institutions who kicked-started the development of Vortex-Lattice Methods for the calculation of aerodynamic bodies which can be found in Margason et al. [11].

The difference between the lifting-line theory and the Vortex-Lattice Method is that instead of one algebraic equation there is a linear system of equations. Also, the bounded vertex is placed at the 1/4 line of each panel while the collocation point is placed at the 3/4 line as shown in Figure 8. There is no mathematical derivation for that, rather it is simply a rule of thumb which works well, first discovered by the Italian Pistolesi. The system of linear equations is:

$$\begin{bmatrix} V_{1,1} & \cdots & V_{1,m} \\ \vdots & \ddots & \vdots \\ V_{n,1} & \cdots & V_{n,m} \end{bmatrix} \begin{bmatrix} \Gamma_1 \\ \vdots \\ \Gamma_n \end{bmatrix} = \begin{bmatrix} b_1 \\ \vdots \\ b_n \end{bmatrix} \tag{3.6}$$
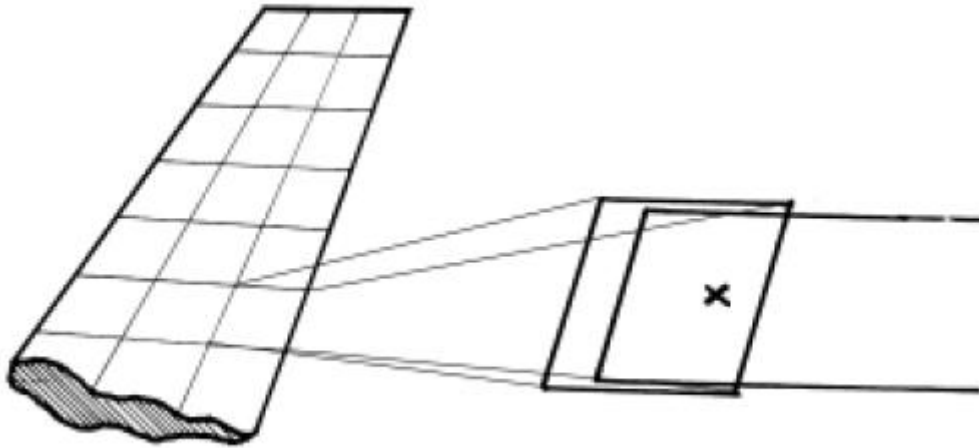
Figure 8

Here, $V_{n,m}$ is the induced velocity at each panel and the boundary conditions are placed in the vector on the right hand side of the equation. In this case, the Neumann boundary condition is applied which states that the normal velocity component is zero at the collocation points. By applying that boundary condition it ensures that the flow cannot penetrate a solid wall i.e. in this case the wing surface. It is possible to solve this linear system of equations and to obtain the value for Γ at each panel. By further applying the Kutta-Joukowski-theorem which is given in equation (3.7) it is possible to calculate the lift at each panel.

$$L = \rho U_\infty \Gamma \qquad (3.7)$$

The summation of all lift components at each panel yields the overall lift. Having calculated the overall lift, it is possible to derive the lift coefficient.

That is the main principle of the Vortex-Lattice Method. It is important to know that the main idea is derived from the Navier-Stokes equations. The full set of the Navier-Stokes equations are non-linear, partial differential equations of second order, not solvable in an analytical manner so far. By neglecting some effects of the flow such as viscosity, rotation and compressibility it is possible to solve the equations. In this case, the Navier-Stokes equations are reduced to a potential flow problem which has become linear and a partial differential equation of first order. There are however many ways to expand this method to achieve a more complex solution. For example by applying a boundary layer method is also possible to approximate the drag. A classical work book on that topic has been published by Katz et al. [12] that discusses various numerical techniques to obtain aerodynamic coefficients for easy and more sophisticated cases.

3.2. TORNADO – A free Vortex-Lattice code for MATLAB

It is beyond the scope of this work to develop an own Vortex-Lattice Method in order to evaluate different wingtip designs. Also, it is not necessary since other programs, published under free licenses are widely available. For the following work the program called "TORNADO", developed by

Tomas Melin in 2000 as part of his master thesis will be used. It distinguishes itself from other programs by its simple user interface yet very powerful evaluation capability. It is possible to add data to the database such as user defined airfoils if desired and the code can even be changed or modified. The latter is not a trivial thing to do since one has to understand the code first which consists of a vast of files.

A very brief instruction is given on the developer's website which is enough to understand the workflow of TORNADO. What makes it so powerful is the fact that it can calculate any arbitrary, three-dimensional shape. There are no restrictions to the geometrical shape however it becomes very difficult to model curved surfaces. If curvature can be neglected and the desired body can be built from different, planar surfaces, it is very easy and fast to model complex geometries which make this program perfect for a preliminary design tool.

Some restrictions have to be taken into account while using TORNADO. Since the equations used are a potential flow in nature it is independent of the Reynolds number. Also it should only be used for incompressible flows. It is possible to activate the Prandtl-Glauert rule to account for compressible flows but this should only be used for two dimensional flows. It is however a good approximation for three dimensional flows as well. Further no information of the thickness of an airfoil is needed for the calculation of the lift. There is no difference between a NACA 2408 and NACA 2412 airfoil since only the camber line is taken into account for calculation. Further information about the program can be found in Melin [13] or in Schiktanz [14].

4.2.1   The workflow in TORNADO

First of all, all the necessary MATLAB files to get TORNADO running have to be downloaded from http://www.redhammer.se/tornado/ (last checked 28.04.2012). It comes in a zip archive and can be extracted anywhere on a PC. Once that is done it can be started out of MATLAB. All that one has to do is to start MATLAB, change the working directory to where the TORNADO files are located and type "Tornado" in the command window. The following menu will start to appear on the screen:

- program start -

_____

 TORNADO Version 135 Release version

 build 2010 03 20 14:07 UTC

 Main Menu

_____

 Input operations.

       [1]. Aircraft geometry setup

       [2]. Flight condition setup

       [3]. Change rudder setting

       [4]. Move reference point

 Lattice operations.

       [5]. Generate lattice.

 Computation operations.

       [6]. Processor access

 Post processing and interactive operations.

       [7]. Post processing, Result/Plot functions

       [8]. Keyboard access

 Auxiliary operations.

       [10]. About / Release Info

       [100]. Help files

       [0]. Exit Tornado
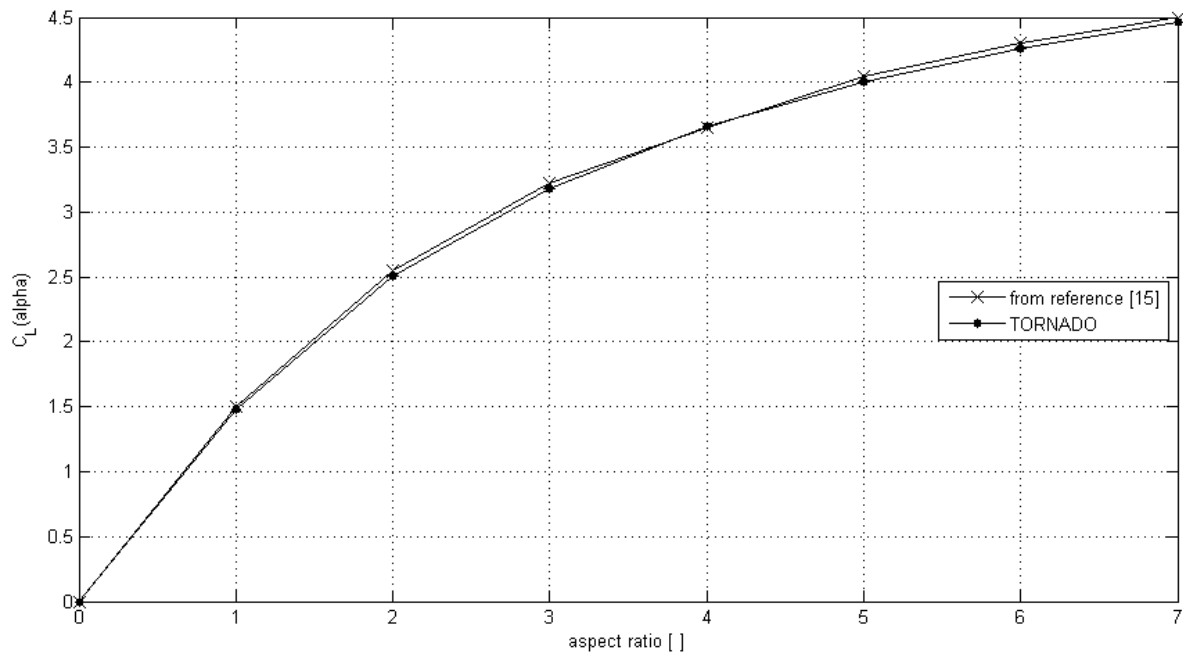
Figure 9

To access the menu one simply has to type the number into the command window. For a simple flow analysis the geometry is defined under [1]. Aircraft geometry setup. Here all relevant data for the geometry is entered into the program. Once that is done, the flight conditions have to be set under [2]. Flight condition setup. In the next step the lattice is generate under [5]. Generate lattice. The case is now set up and can be analyzed. In [6]. Processor access there are a several possibilities to what can be analyzed which forms the powerful core of this program. Not only is it capable of doing the standard static computation which will be used exclusively in the present investigation but also TORNADO is capable of approximating the viscous drag that allows to find the drag polar and it can find the stall angle of attack. Each computation is given a job identity tag (JID) under which the computation will be saved and accessed under [7]. Post processing, Result/Plot functions once the calculation is done.

The results can be conveniently accessed by the plot function that gives several plots holding information for the aerodynamic coefficients, bending moment, forces and cp values or one can access the raw data directly. It is necessary to end the program first. Afterwards the output folder can be accessed where all computations are saved that have been done before under the job identity tag. The data is stored in the internal MATLAB array editor and in the results section every result is stored either as a scalar (such as the aerodynamic coefficients) or in a vector or a matrix (such as the strength of the circulation for each panel). In some cases it is necessary to obtain those results for further analyses as will be addressed in subsection 0.
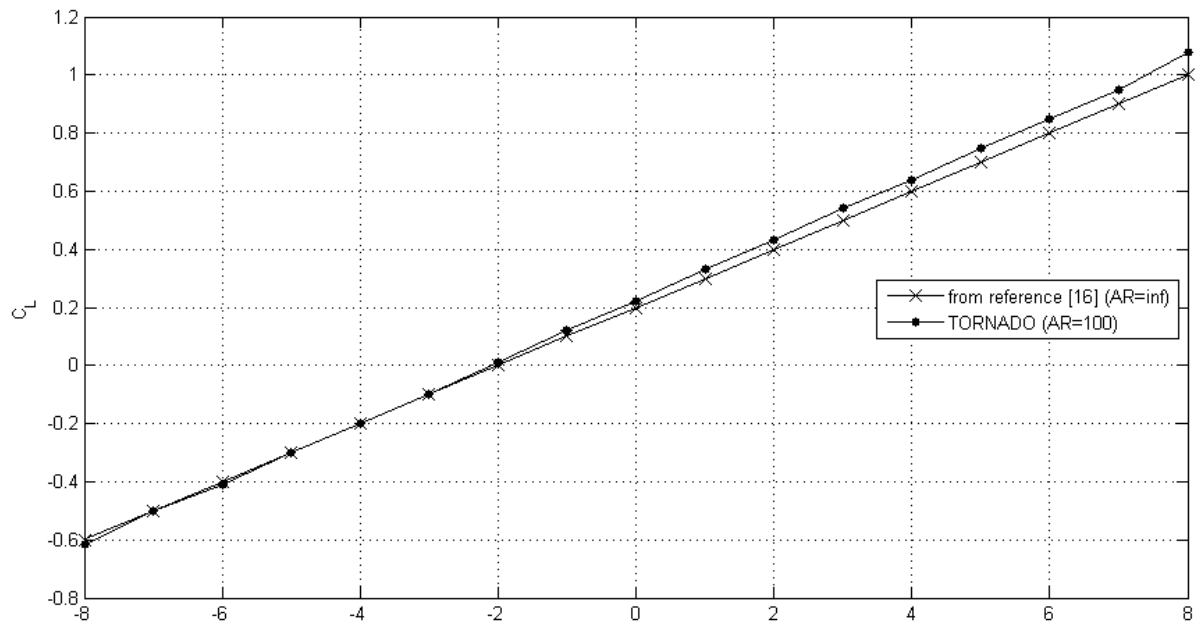
Figure 10

4.2.2   Validation of the TORNADO code

To gain confidence in the TORNADO code it is recommended to perform a validation before using the program further. For that purpose an existing Vortex-Lattice code has been used which already has been tested and validated [15]. For a given wing geometry in that report the slope of the lift coefficient is plotted against the aspect ratio as can be seen in Figure 9. Also the results obtained in TORNADO are plotted. This comparison shows that there is a good conformity which indicates that the code works properly and that there are no errors in the code. That however is not sufficient enough since it does not validate the aerodynamic conclusiveness. For that reason a wing with an aspect ratio of Λ=100 and a NACA 2412 airfoil was tested. Since TORNADO is only capable of calculating 3D geometries a large aspect ratio has to be taken in order to approximate a two dimensional case. Once it can be seen as two dimensional it can be compared with the data from Abbott and Doenhoff [16]. Also, only the linear range of the slope of the lift coefficient is taken since TORNADO uses the potential flow to calculate the lift capabilities. As can be seen from Figure 10 there is again a good conformity. It can be expected that TORNADO works well for the range that it has been developed for, making it a good tool for the preliminary investigation.

3.3.   The optimum wingtip configuration

By studying the literature available it is clear that there is no general equation to describe the optimum wingtip design. First of all it has to be clear from which standpoint the wingtip should be optimized. By trying to find an optimum aerodynamic design there is always a conflict between aerodynamic and structure. Each wingtip modification changes the pressure distribution and eventually the bending moment at the root which leads to a higher structural mass at the wing root. So it is hardly possible to evaluate the aerodynamic benefits without looking at the bending
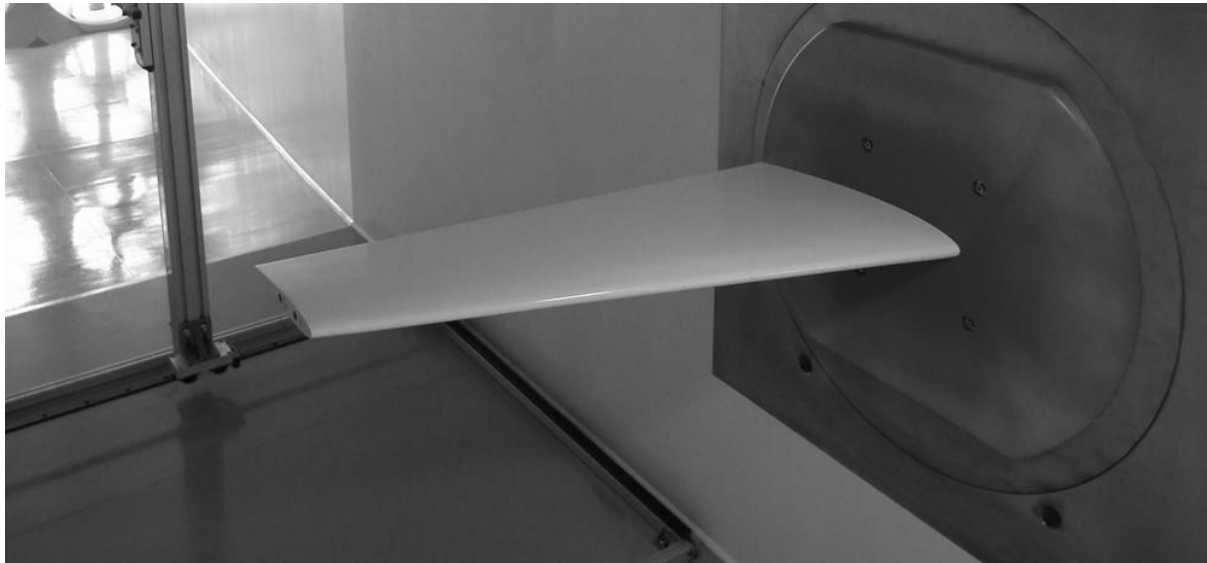
Figure 11

moment. Since it is just as easy to extract the bending moment at the wing root in TORNADO as it is to extract the lift coefficient for the wing, the bending moment will be observed but will not be the primary parameter to assess whether a configuration is better than the clean wing without a wingtip modification or not. Due to the direct relation between lift and bending moment it will be considered. No further result, not directly related to aerodynamic will be assessed however. Even with a straight optimization goal in mind it is still not possible to apply some rule of thumbs or equations to get fast to a solution. Each wing needs its own wingtip design and the same wingtip design may not work on a different wing. As mentioned by Whitcomb it is easier to worsen the flow field around the wingtip than to improve it.

To sum it up, first the optimization goal has to be defined (in this case an aerodynamic optimization) and then the optimum design has to be found for a given wing configuration.

The wing that will be used in the present investigation is shown in Figure 11. For an optimization the wing has to be investigated first without any wingtip modification in order to lay some groundwork for the further comparison. For the investigation an incompressible flow at a free-stream velocity of 10 m/s and an angle of attack of 5° has been defined. The data for the wing can be taken from Table 2:

Wing Parameter	Value
Length of chord at wing root	427.43 mm
Length of chord at wing tip	228 mm
Span	858 mm
Taper ratio	0.533
Aspect ratio (for a symmetrical wing)	5.5
Sweep angle	18.2°
Airfoil wing root	NACA 0013
Airfoil wing tip	NACA 0013

Table 2
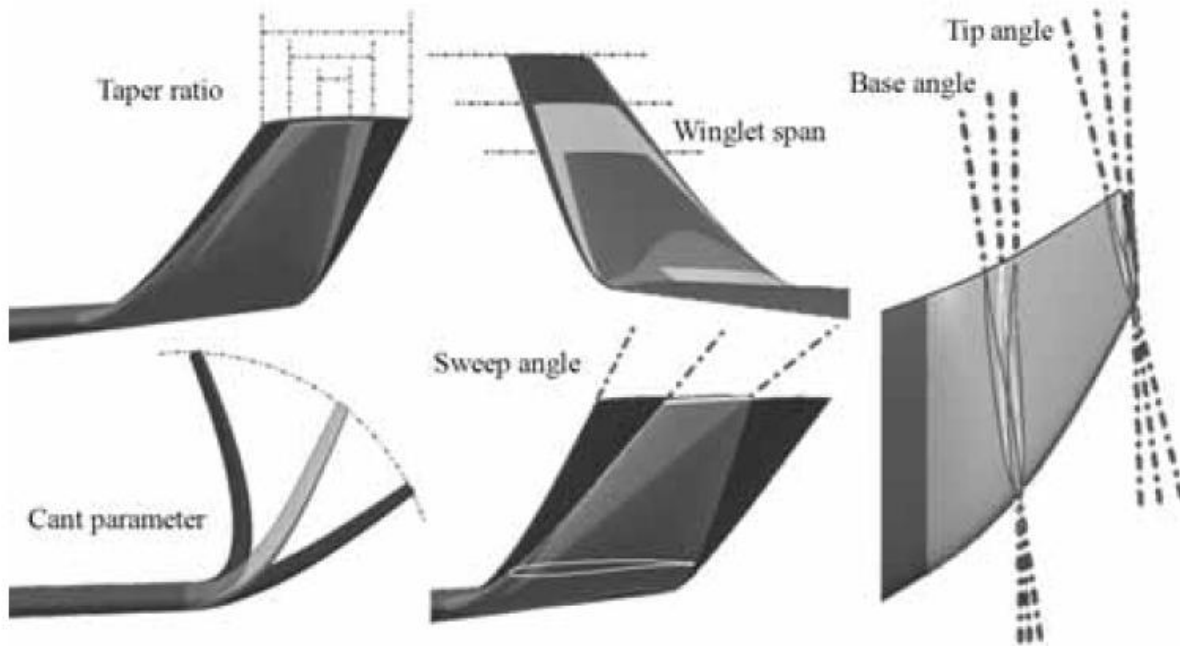
Figure 12

4.2.3   The winglet configuration

At first glance, a winglet might appear as a simple span augmentation that is canted upwards. That may be but there is more to it than meets the naked eye. In Figure 12 the 5 main design parameters are shown:

- Span: The span of the winglet is defined as the distance from the winglet root to the winglet tip. In case of a blended winglet the junction between the winglet itself and the main wing is considered to be part of the winglet. Therefore the winglet span should not be confused with the winglet height however when modeling the winglet geometry in TORNADO with planar surfaces the height and span are the same.
- Wing tip to winglet root relation (not shown in the picture): As it says, it is the relation of the wing tip to the winglet root. By making the winglet root smaller than the wing tip and thus placing the winglet further aft while the trailing edge will remain a straight line. It is said that this will reduce the aerodynamic interferences [9].
- Taper ratio: It is defined as the relation between the winglet tip to the winglet root as:

$$\lambda = \frac{c_{tip}}{c_{root}}$$
(3.8)

It is the same definition as for the wing. The taper ratio should not differ too much from that of the main wing.

winglet normal force

reduced bending

increased bending
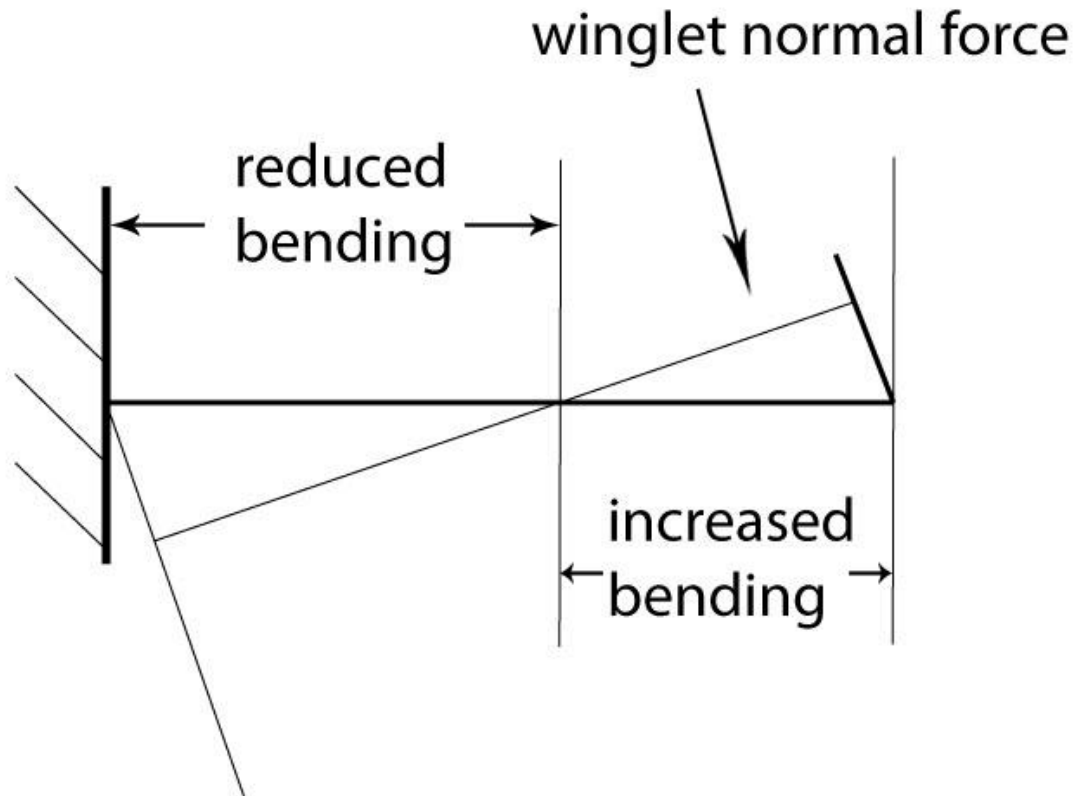
- Sweep angle: It is measured at the quarter line of the wing and should be of the same magnitude as the main wing but slightly higher in order to increase the critical Mach number, a rule of thumb is:

$$Ma_{crit_{Winglet}} = Ma_{crit_{Wing}} + 0.01 \qquad (3.9)$$

- Cant angle: It is the angle by which the winglet is canted upwards. It is measured from the plane in which the main wing is to the winglet. A cant angle of 90° transfers to a vertical winglet. A cant angle greater than 90° can reduce the root bending moment as shown in Figure 13 but reduces the effectiveness when it comes to reduce the induced drag.
- Twist angle: There are two twist angle, one at the winglet root and one at the winglet tip. The twist angle is used to achieve the same stall characteristics on the winglet as on the main wing. That means that the winglet should not stall before the main wing.

In order to find the optimum design, it would take too long to investigate all possible parameter combinations since TORNADO is not made for automation. That means that each parameter combination has to be generated manually and checked after the calculation. As mentioned before it is possible to access the code but it would simply take too long to understand and rewrite the code until it is capable of investigating all parameter combination automatically. However, some simplifications can be made which reduces the number of calculations.

Since the design process is carried out for an incompressible case, the sweep angle and hence the critical Mach number is of no important role. Therefore it was kept roughly at the same value and just increased slightly due to a round off to the next higher number. From wing theory it is known that a trapezoid wing with a taper ratio of 0.45 yields a nearly elliptical lift distribution. Therefore 0.45 is set for the taper ratio and not changed for further investigations.

The twist angle is something which is possible to obtain from potential flow, even if the knowledge of the stall angle and therefore of viscous effects are required. The lift coefficient can be obtained by the pressure distribution from:

$$C_L = \frac{1}{c} \int_0^c \Delta C_p \, dx \qquad (3.10)$$

If the maximum value for C_L for winglet airfoil is of the same order of the main wing then it has to be expected that the winglet will stall before the main wing due to the superimposed flow at the wingtip as discussed earlier. Therefore a slightly outward twisting is required to overcome this problem and achieve similar stall characteristics.

The values for the difference in the pressure coefficients can be obtained directly from TORNADO on each panel. Integrating those values along the chord yields the local C_L value. The maximum C_L value for a given airfoil can be looked up in airfoil databases. If the integrated value for C_L is greater than the maximum value a stall will be triggered at that point. By twisting the winglet outwards the inflow angle will be reduced and eventually a stall avoided.

For the further investigation the influence of the winglet span, cant angle and wing tip to winglet root relation will be investigated and the simplifications mentioned before applied.

4.2.4   The raked wingtip configuration

As mentioned before by Whitcomb, it is easier to worsen the wingtip situation with a winglet than without it. That is why several iterations with different configurations have to be tested. This can however not be said for the raked wingtip in general. The raked wingtip works as a span augmentation, having a special appearance compared to a normal span augmentation. For that reason it is possible to derive more generalized design requirements for the raked wingtip. The US patent 6,089,502 [3] gives specific design guidance which is incorporated for the following design. The most important one are discussed below:

- Span: It is mentioned in the US patent that the span should range from 6 – 12 % of the main wing span. Also it is said that the higher span augmentation yields the best results.
- Taper ratio: The taper ratio should be set to a low value. In this way the crossflow at the tip will be reduced.
- Sweep angle: The US patent referred to the sweep angle at the leading edge, not as usual to the quarter line. For sweep angles of 40 – 50° high lift devices such as slats are required to overcome the premature stall characteristics. In the case of more sweep angle between 50 - 60° the premature stall vanishes and no slats are required, yielding less structural weight.

- Airfoil: A symmetrical airfoil should be used. This reduces the lift force and pressure distribution on the raked wingtip and therefore the root bending moment and the crossflow at the tip.

In this case the length of the raked wingtip is equal to 20% of the overall span of the main wing (one wing, or 10% for a symmetrical wing). The taper ratio is set to 0.1 and the sweep angle is set to 57°. For the taper ratio this seems to be a good value while the sweep angle is explicitly given in the US patent [3]. To match the airfoils already used on the main wing, a NACA 0013 airfoil is applied for the whole raked wingtip. Therefore the design of the raked wingtip is already given, based heavily on the US patent and it will be tested against the winglet design which will be found after the iteration process.

3.4. Results

In the following the results will be presented and discussed which have been obtained by using TORNADO. The first flow property obtained is the lift coefficient and it is calculated as:

$$C_L = \frac{L}{\frac{1}{2}\rho U_\infty^2 S_{ref}} \tag{3.11}$$

with S_{ref} being the reference area of the wing plus wingtip configuration. The induced drag is obtained by applying the Trefftz-plane analyze which is discussed in detail in section 7.4.2. The root bending moment coefficient is defined as:

$$C_B = \frac{M_r}{\frac{1}{2}\rho U_\infty^2 S_{ref} c_{MAC}} \tag{3.12}$$

with M_r being the root bending moment and c_{MAC} the mean aerodynamic chord of the wing. Further the slope of the lift coefficient i.e. $C_L(\alpha)$ is observed.

The first results are the values obtained for the clean wing without any wingtip modification. They are given in Table 3 and will be used for the comparison against the winglet and raked wingtip design:

Clean Wing with no wingtip modification				
	C_L	$C_L(\alpha)$	C_B	$C_{D,i}$
NACA 0013	0,255	2,911	-0,313	0,0079

Table 3

Four different airfoils were investigated for the winglet configuration:

1. NACA 2408
2. PSU 90-125
3. NACA LS(1)-0413
4. Whitcomb's winglet design

The NACA 2408 is a thin, cambered airfoil and is taken as a representative for the NACA airfoil family. The PSU 90-125 airfoil is the most used airfoil for winglets on sailplanes, designed by Mark D. Maughmer and is promising since it is used for incompressible flight condition, although for wings with a high aspect ratio. The NACA LS(1)-0413 is taken from [17] as suggested by Whitcomb in his report. Finally, the Whitcomb design itself is taken. The airfoil name is not mentioned but the airfoil coordinates are given and could be implemented in TORNADO. The results for the four different airfoils are given in Table 4:

Wing plus winglet configuration				
	C_L	$C_L(\alpha)$	C_B	$C_{D,i}$
NACA 2408	0,243	3,2694	-0,326	0,0054
PSU 90-125	0,247	3,2403	-0,325	0,0055
NACA LS(1)-0413	0,251	3,2431	-0,327	0,0056
Whitcomb	0,252	3,2441	-0,327	0,0057

Table 4

As mentioned before there will be just one airfoil to be investigated for the raked wingtip. The results are given in Table 5:

Wing plus raked wingtip configuration				
	C_L	$C_L(\alpha)$	C_B	$C_{D,i}$
NACA 0013	0,267	3,480	-0,324	0,0069

Table 5

The reduction or increase is given in Table 6 for both the winglet and the raked wingtip configuration:

Comparison of winglet and raked wingtip configuration to main wing				
	C_L	$C_L(\alpha)$	C_B	$C_{D,i}$
Winglet:				
NACA 2408	-4,96%	10,94%	4,04%	-32,3%
PSU 90-125	-3,14%	10,14%	3,85%	-31,1%
NACA LS(1)-0413	-1,74%	10,22%	4,28%	-29,1%
Whitcomb	-1,27%	10,25%	4,43%	-28,4%
Raked wingtip:				
NACA 0013	4,53%	16,34%	3,42%	-13,2%

Table 6

A decrease in the lift coefficient is reported for all winglet configurations. This is rather strange since it is expected that the winglet increases the lift on the main wing due to the fence like effect. However it has to be kept in mind that the aspect ratio is relatively low thus making the winglet in comparison to the wing very big. The new lift coefficient is calculated using a new reference area,

consisting of the wing surface and winglet surface area. For that reason a reduction is observed. The overall lift however is increased in all cases as expected. Details can be found in Appendix A.

One of the ideas is to reduce the size of the winglet. What is observed in the iteration process is that the lift coefficient decreases with an increase in winglet height. So a minimum in reduction in terms of lift coefficient but a maximum reduction in terms of induced drag has to be found. In this case, the winglet height has an optimum for the same value as the length of the wingtip of the main wing. From Table 4 and Table 5 the values corresponding to the optimum design are given both for the winglets and the raked wingtip. The induced drag has reduced in all cases. Looking at the results the NACA 2408 airfoil produces the best results. The PSU 90-125 airfoil performs quite well as well as the NACA LS(1)-0413 and the Whitcomb airfoil but they are not able to outpace the NACA 2408 airfoil in reducing the induced drag. Since that is the main goal that should be achieved the NACA 2408 is taken for further investigations. The raked wingtip is capable of increasing the lift coefficient. That is no surprise since it can be seen as well as a span augmentation, just having a special shape. Also the raked wingtip improves better on the slope of the lift coefficient. But the real improvement is the reduction in root bending moment compared to the winglet design. In this case it is not relevant since only the aerodynamics are assessed but this difference in bending moment reduces the structural mass at the wing root thus increasing the efficiency of an airplane in a different manner. However it is not as good as the winglet when it comes to reduce the induced drag.

What can be taken from Table 6 is the fact that the winglet is mostly concerned in optimizing the aerodynamics while the raked wingtip tries to improve on several aspects such as aerodynamics and structural aspects. That makes it very difficult to compare the winglet with the raked wingtip further. However it will be still possible to make a fairly good comparison of those two designs keeping in mind that the raked wingtip is a multi dimensional optimization in nature.

In the last step the stall characteristics for the winglet design have to be optimized. Therefore the stall angle for the main wing is found. TORNADO is capable of finding the stall angle by using the same technique discussed in section 0. Once that is determined, the stall angle can be found on the winglet by evaluating equation (3.10) at each panel for different twist angels at the winglet root. The stall angle of the main wing is found to be 15.8° while that directly correspond to a twist angle of 3° outwards. Now that the final configuration has been found for the winglet design, one final calculation has to be done with the new twist angle and is reported in Table 7:

Wing plus winglet configuration with new twist angle of 3° at winglet root				
	C_L	$C_L(\alpha)$	C_B	$C_{D,i}$
NACA 2408	0,265	3,1365	-0,324	0,0057

Table 7

It is not possible to optimize the stall characteristics for the raked wingtip design for the following two reasons:

1. A twist angle at the raked wingtip root would lead to a jump at the junction of the wing and raked wingtip.
2. A further sweep back of the leading edge would compromise the overall effectiveness of the raked wingtip. The sweep angle of 57° at the leading edge is already at the limit. Everything closer to 90° would increase the crossflow again.
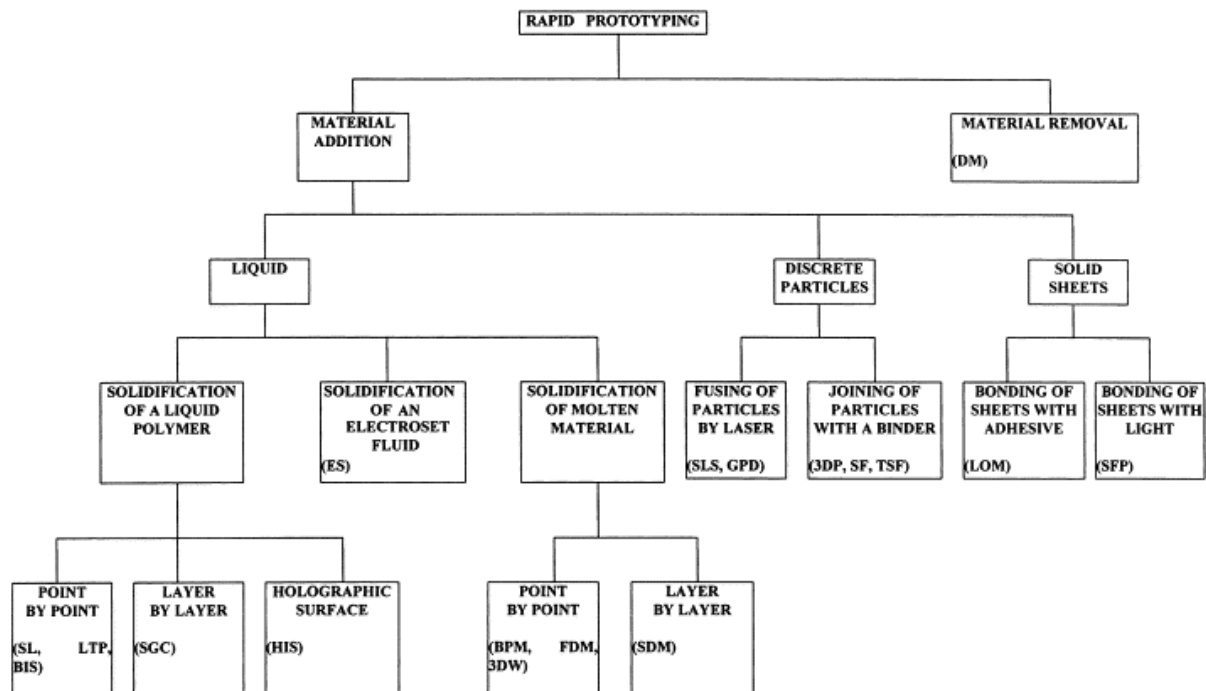
Figure 14

For those reason the stall characteristics are already set. However the stall is investigated on the raked wingtip for an angle of attack of 15.8° and there are already zones where a stall has to be expected. This compares good with the flow visualization tests that have been undertaken by Herrick et al. [3]. However it is also reported that the overall take-off climb drag is reduced with the current design by as much as 5%, at a stage, where the highest angle of attacks are to be expected. In this manner, the premature stall that is triggered by high angle of attacks does not play a very important role.

That concludes the preliminary investigation. For the further investigation the winglet with the NACA 2408 airfoil has been selected and will be compared against the raked wingtip as mentioned in the US patent. The detailed geometry will be discussed in chapter 4.2.

4. Detailed design

4.1. Rapid prototyping

Before a detailed design in CATA can be achieved it is mandatory to know how the final part will be manufactured. In this case the rapid prototyping technology will be used. It offers great advantages compared to conventional manufacturing processes but comes with some disadvantages which have to be considered in the designing process.

Rapid prototyping was invented in 1986 by 3D-Systems. The first Rapid prototyping technology ever used was the Stereolithography (SLA). Since then there has been a great development. Nowadays, engineers have a broad spectrum of rapid prototyping solutions which they can choose from. Figure 14 gives an overview of different technologies available today.

Figure 15

In general, rapid prototyping (often referred to as 3D printing) is the process of printing a CAD model layer by layer. By that it is possible to have a physical prototype rather than just a computer model in an early design stage. Design flaws and errors are s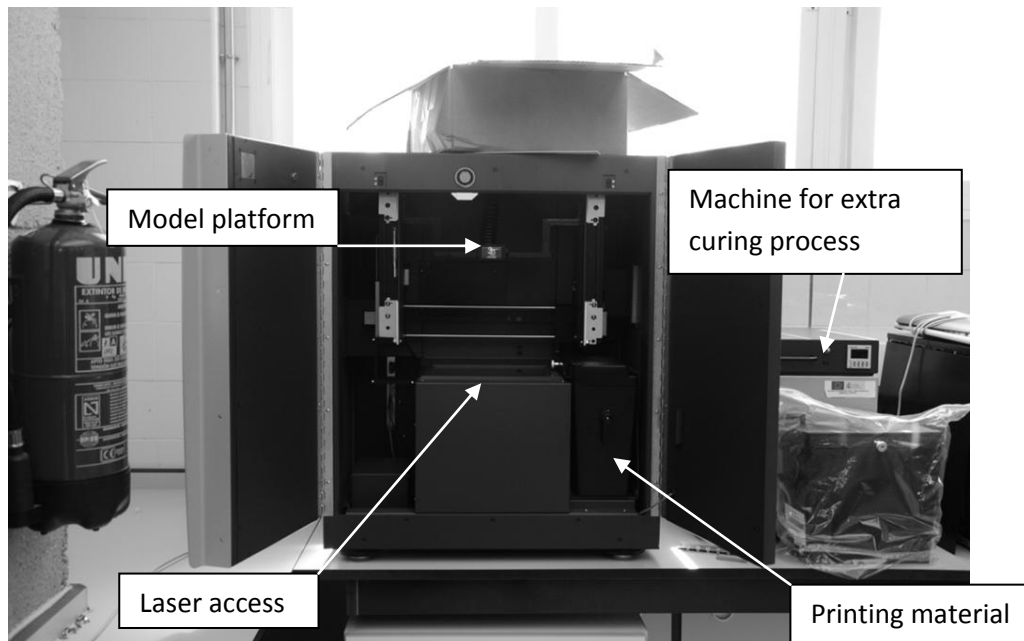potted easily and can be eliminated, thereby reducing costly mistakes. Usually the parts are made out of materials which do not have sufficient strength to place them in an assembly. However there have been developments to overcome this weakness e.g. the selective-laser-sintering (SLS). It has to be kept in mind that rapid prototyping is meant to be for single part manufacturing (prototypes) and therefore it is not feasible to have a large-scale production due to the time penalty. Still, it is one of the best technologies available today when it comes to constructing complex geometries with high accuracy.

The process of rapid prototyping can be described as the following:

1. A CAD model is constructed and then converted into the *.stl format. This format divides the whole surface of the part into triangles. The position at each corner is saved in terms of coordinates as well as the vector normal to the surface.
2. The rapid prototype machine reads the *.stl file and creates a model which is made out of layers. Each layer is usually 0.1 mm thick, depending on the accuracy of the machine and user inputs.
3. The first layer is build. After that is done the platform where the model is printed lowers and a second layer is printed. This process is repeated until the last layer is printed.
4. The model is taken from the machine, cleaned, support structures are removed and the part is healed if necessary.

For the following investigation the Vflash machine from 3D Systems is used which uses the Stereolithography technology in a slight modified way. A picture of the machine is given in Figure 15 and an introducing video to the machine is given on the CD. For details refer to Appendix A.

The Stereolithography is inexpensive when compared to other rapid prototyping technologies. It uses a light-sensitive liquid polymer that becomes solid when in contact with laser. One of the

disadvantages is that the laser is not strong enough to cure the part completely. For that reason the part is still weak during the building process. That can be particularly a problem since the Vflash machine, in contrast to other 3D printer, builds its model hanging from a platform at the ceiling rather than staying on a platform on the floor. Each added layer will increase the mass and therefore the bending moment at the models root if the center of gravity is not located in the middle of the part. This will cause the model to bend which affects the overall quality. To minimize that problem, the model has to be built out of as little material as possible but as much material as needed in order the withstand the force that will be exerted on it during the wind tunnel tests. That problem will be tackled in the next section in detail.

Once the part has been printed it has to be removed from the machine and cured as described above. In detail, the steps are:

1. The model is removed from the printer. At any time gloves must be worn.
2. The model is washed in a tank of chemicals for five minutes and then in a tank of water for five minutes.
3. Drying the model with a hair dryer. Removing as much liquid as possible.
4. The part is cured in another machine. The time depends on the size and shape of the part.
5. The support structures are removed.
6. The part has to be cured another time. Several curing sessions may be done for complex geometries to expose all of the surfaces.
7. Final tooling can be done on the part. For aerodynamic shapes the surfaces are sanded with a fine sand paper to give it a smooth surface.

After those seven steps the part is completed and can be used for further analysis.

4.2. Design considerations in CATIA

As mentioned before it is not feasible to print the wingtip devices as a filled volume part, rather hollow spaces have to be incorporated not only to reduce the bending moment but also to minimize the usage of the expensive material used for printing.

The first problem is the main wing itself. Both designs, the winglet and the raked wingtip, have to be fitted on the existing wing which is shown in **Fehler! Verweisquelle konnte nicht gefunden werden.** without any wingtip devices. Originally it was built with NACA 0012 airfoils at each span location but due to coating the relative thickness at the wing root is 13.1% and at the wing tip 12.9% therefore consisting more or less of NACA 0013 airfoils. Also the shape of the airfoil differs slightly from that of a NACA 0013 at the wingtip. In order to determine the exact shape a 3D scan was done at the wingtip. The data are converted into a step file (*.stp) which can be opened in CATIA.

The scanned airfoil shows good comparison at the leading edge where the most deviations are located in comparison to the NACA 0013 airfoil. Despite the good resolution for the highly curved part at the front, the scanner has problems to resolve the part around the trailing edge with nearly no curvature. The sign of the curvature even changes from location to location. The inbuilt curve smoothing feature in CATIA is of no help to resolve that problem. Therefore a hybrid airfoil is designed, taken the good leading edge region from the scan and the smooth trailing edge region
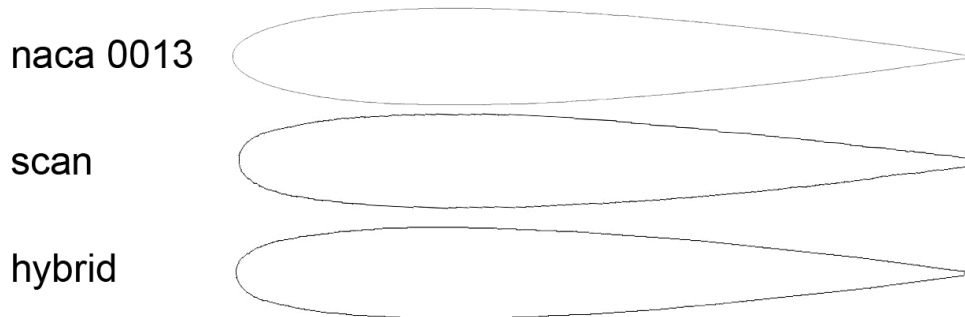
naca 0013

scan

hybrid

from a NACA 0013 airfoil. The gap in the middle is connected via splines each being tangential at the connection points. A NACA 0013, the scanned and the final hybrid airfoil is shown in Figure 16. The main differences can be spotted at the trailing and leading edge by a close inspection. Part specific thoughts for the design process are given bellow. They are in order by which they have been designed and constructed. In that manner it is easier to understand which changes have been made in order to improve the next part.

5.2.1   Clean wing extension

The adjacent surface at the wingtip to the chord line is a rather unusable surface for wind tunnel testing. It has a rough surface texture while it holds holes for attaching other wingtip devices. It was decided that it would be best to cover this part with a wing extension. The decision to print a wing extension rather than tooling on the wings wingtip provides the opportunity to design a simple part from which mistakes can be spotted and avoided for the winglet and raked wingtip design.

The main concern is how to fit the extension onto the wing which is a crucial design factor for the other designs. The most straightforward solution is to implement two holes on the upper surface which give space to access the screws once they have been in place. The problem then is to cover the holes. Two doors must be constructed to cover the holes, however since there is no locking mechanism for the doors it can be expected that they would just stay too loosely on place. The best way to overcome this problem is to cover the doors with a strip of tape. The tape however has a different surface than the wing and the wing extension which will influence the flow at the wingtip.

There is a different, more sophisticated design which allows the wing extension to slide into position and lock itself, therefore getting rid of the holes, but it is too complex. It is likely that the printer is not able to resolve the geometry fine enough at locations of importance in order to make this design work. So the originally idea is taken.

The Part itself is 50 mm long and follows the trailing and leading edge. An overall thickness of 3 mm is applied for the skin and is used for all designs. The inside is hollow except for some ribs which run nearly parallel to the leading edge. The ribs were not only used for stability reasons, they are an effective yet simple way to influence the location of the center of gravity. By that, the center of gravity is just 1.8% off the centerline of the part. Hence, the influence of bending moments onto the parts can be kept at a minimum.

Figure 17

The final part, mounted to the wing, is given in Figure 17 (note that the tape is not visible here).

5.2.2   Raked wingtip

The initial impression from the wing extension was acceptable so no major changes were made for the raked wingtip. The ribs are located at the same spots as before on the wing extension and are following a similar curvature of the leading edge. There have been some changes but only due to stability reasons. The total height at the tip of the raked wingtip is approximately 3mm so the last third of the part is filled with solid material to strengthen the structure. The door concept has been renewed. There is just one big door instead of two small ones. What could be seen from the first try is that the doors where so tiny that the printer had problems to give them the right curvature. Making a bigger door should not only ensure a better resolution of the curvature but also gives more space to adjust the screws more easily. Again, as on the wing extension, tape is used to hold the door in place. The final part is given in Figure 18.

Figure 18

Figure 19

5.2.3   Winglet

The winglet has been constructed at a much later stage than the raked wingtip. Due to that reason, long-term observation has shown that small buckles are to be found on both the wing extension and the raked wingtip surface. To address this problem the inside of the Winglet was constructed with additional structure to support the surface. This structure and the final design is shown in Figure 19. The Winglet itself is beyond the printable range of the printer so it has to be printed in two parts. One part resembles the curved part that is mounted onto the wing. The second part is the canted wing itself. Extra material is added to the Parts where there are surfaces which are later used for connecting to pieces. The extra material is then sanded-off to ensure a smooth surface and finally they are glued together.

During the build process the printer automatically places support structure where needed in order to ensure that the part that is printed does not bend to one side as well as to support its weight. That has not been a problem before since all parts have been straight parts so the only support structures were placed at the surface that has been the connection between the wing tip devices and the wing itself. For the winglet however that is not true anymore. The curved part of the winglet has to be placed in such a way that at least one surface will be affected. This cannot be avoided and has to be taken care of in the sanding-off process.

As mentioned before in chapter 4.2.3 " The winglet configuration" the stall on the winglet should be triggered after the stall on the main wing. To achieve that the Winglet has to be twisted outward with an angle of 3°.

All designs are included as CATIA file format (CATIA V5 R20) in Appendix A. Further, technical drawings are attached in Appendix B with relevant aerodynamic data.

5.   Numerical Investigation

5.1.   Purpose of CFD investigations

The general purpose of computational fluid dynamic (CFD) simulations is to get a better understanding onto what is going on in the flow field. Sometimes there are areas in the flow domain where measurements are hard to take which values are in turn easy to obtain from the CFD simulation. Experiences on the last decades have shown that it is a good practice to compare CFD values against wind tunnel data whenever possible. Also, if both resources are available, it is beneficial to use the data obtained in both the wind tunnel experiment and the CFD simulation to validate the results thus reducing errors and to gain more confidence in the actual results.

Sometimes it is also very helpful to choose either a wind tunnel experiment or a CFD simulation by the type of simulation that should be conducted. The table given below states the pros and cons of each method.

Wind tunnel	
Pro	Con
Real flow domain	Wind tunnel geometry influence results
All aspects of the flow are covered (Turbulence, flow separation etc.)	Measurements are hard to obtain in some regions
Quick way of obtaining results	For each test a model has to be build or adjusted
CFD simulation	
Pro	Con
Results easily accessible	Modeling and mesh dependency studies take time
Parametric study easily possible	Huge computational time needed for engineering applications
Complex geometries can be simulated	Broad knowledge of CFD needed in order to avoid input errors

Table 8

A parametric study therefore might be best done in the CFD simulation, however, if the investigated model can be adjusted easily than the wind tunnel testing time could be significantly smaller than the computational time.

In the present investigation all three wing configuration will be tested in the wind tunnel and in a CFD simulation. The obtained results will then be compared against each other and against the results obtained in TORNADO.

5.2.   Numerical model

The set of the full Navier Stokes equation, namely the continuum, momentum and energy equation, are given in (5.1) to (5.3). Before a numerical simulation is done it is useful to consider which part of the flow should be captured and which part can be neglected. In that way the Navier-Stokes equation can be reduced to save computational time.

$$\frac{D\rho}{Dt} + \rho \nabla \cdot U = 0 \tag{5.1}$$

$$\rho \frac{DU}{Dt} = \rho g - \nabla p + \mu \nabla^2 U \tag{5.2}$$

$$\rho \frac{D\left(e_0 + \frac{U^2}{2}\right)}{Dt} = \rho \dot{q} - \nabla \cdot (pU) + \rho(f \cdot U) \tag{5.3}$$

The first assumption that can be made depends whether compressibility or incompressibility should be considered i.e. is the winglet / raked wingtip designed for a large commercial airplane at subsonic speed or should it be optimized for smaller aircrafts below 0.3 Ma. In the following investigation the flow is regarded as incompressible due to the aspect ratio of the wing which falls in the range of a small aircraft and the wind tunnel itself which is a low speed wind tunnel. Therefore the energy equation can be neglected and is not considered further.

The main focus is to obtain the induced drag coefficient. Therefore all information on drag would be extra information of little use at a high time penalty. For that reason the viscosity is neglected (μ=0). By neglecting the term of the viscosity the order of the partial differential equation has dropped to a first order partial differential equation. Neglecting the viscosity yields the Euler equation which is used in the CFD simulation. All calculations are done with the commercial available software FLUENT.

5.3.   Judgment of results

6.3.1   Mesh dependency study

The purpose of a mesh dependency study is to ensure that the CFD simulation is not depending on the mesh. In order to conduct a mesh dependency study three different mesh sizes have to be generated and simulated. To judge the mesh it is mandatory to observe a certain flow property of interest. In this investigation the value of C_L will be taken to judge the dependency of the mesh. The mesh dependency study as well as the iteration error and its uncertainty which will be addressed in the next section are based on a method introduced by Celik et al. [18]. It is the same method that is been used for reporting the accuracy of a numerical simulation in the "Journal of Fluids Engineering"

First, a representative mesh size has to be obtained, for a three dimensional case following Celik this is:

$$h = \left[\frac{1}{N} \sum_{i=1}^{N} (\Delta V_i) \right]^{\frac{1}{3}}$$

(5.4)

h has to be calculated for all three meshes. Then, the ratio of mesh size 1 to 2 and from 2 to 3 can be calculated i.e. r_{21} and r_{32}. The ratio of r should not be less than 1.3. This value is based on experience and not on formal derivation. With the ratio of r the apparent order p_a can be obtained iteratively by:

$$p_a = \frac{1}{\ln (r_{21})} \left| ln \left| \frac{\varepsilon_{32}}{\varepsilon_{21}} \right| + q(p_a) \right|$$

(5.5)

$$q(p_a) = ln \left(\frac{r_{21}^{p_a} - s}{r_{32}^{p_a} - s} \right)$$

(5.6)

$$s = sgn \left(\frac{\varepsilon_{32}}{\varepsilon_{21}} \right)$$

(5.7)

Where $\varepsilon_{32} = \phi_3 - \phi_2$ and $\varepsilon_{21} = \phi_2 - \phi_1$. ϕ is any arbitrary flow property, in this case as mentioned before it will be the value of C_L.

With the now available apparent order p_a it is possible to calculate the extrapolated value of ϕ as:

$$\phi_{ext}^{21} = \frac{r_{21}^{p_a} \phi_1 - \phi_2}{r_{21}^{p_a} - 1}$$

(5.8)

The approximate error e_a^{21} can be expressed as:

$$e_a^{21} = \left| \frac{\phi_1 - \phi_2}{\phi_1} \right|$$

(5.9)

The extrapolated error e_{ext}^{21} can be expressed as:

$$e_{ext}^{21} = \left| \frac{\phi_{ext}^{21} - \phi_1}{\phi_{ext}^{21}} \right|$$

(5.10)

Finally the grid convergence index can be obtained by:

$$GCI_{fine}^{21} = \frac{1.25 e_a^{21}}{r_{21}^{p_a} - 1}$$

(5.11)

Similar, the values for ϕ_{ext}^{32}, e_a^{32}, e_{ext}^{32} and GCI_{fine}^{32} are obtained. The grid convergence index or GCI was originally introduced by Roache [19] and differs slightly from the definition above. It is a way to judge the mesh dependency of a simulation. This value should be as low as possible. The subscribed "fine" is the normal way of obtaining the GCI there is however a way of judging mesh dependencies when a huge amount of calculations on different mesh sizes are done. Then, it is possible to use a coarse grid convergence index which is different compared to the fine one. Details can be found in [19]. For the present investigation a mesh dependency study has been done for the raked wingtip configuration. The knowledge obtained from that was adapted for the clean wing and the winglet mesh. A mesh dependency study should be done for each calculation in theory however due to the time penalty it would cause it is a good approach to make it just for one case and then adopting the mesh details onto the other meshes. The values for the raked wingtip configuration can be found in Appendix C.

6.3.2   Iteration error and uncertainty

In order to judge if a solution has been fully converged or not a different algorithm has to be introduced. The convergence in FLUENT is calculated in terms of the global residuals in the flow domain. This value is not in particular useful since it varies significantly for different conditions. It is calculated by a weight coefficient for the cell l_P times a flow property ϕ_P and then subtracted from the influence of the neighboring cells. To make it a global residual it is divided by $l_P\phi_P$ thus yielding:

$$R^\phi = \frac{\sum_{cellsP} |\sum_{nb} l_{nb}\phi_{nb} + b - l_P\phi_P|}{\sum_{cellsP} |l_P\phi_P|}$$

(5.12)

The subscript P stands for present cell and nb for neighbor cell. The value of b can be regarded as a contribution from a source term and will not be considered further.

The problem is now that the value of the residual depends heavily on user inputs. For example in the case of the flow around a wing which is done in the present investigation, consider the initial guess for the flow domain. Before the CFD calculation can be started it needs a start value at each node of the mesh. Consider an initial guess of zero for all velocity components at each node and consider a second case where the same velocity value as the flow inlet is used for each node. It is obvious that in the first case the residual will drop significantly due to a huge change through the flow domain while it will drop less for the second time since a good initial guess has been found. This shows the problematic nature of the residual which is the reason for another solution to judge convergence. This approach is again based on Celik et al. [18]. The iteration error is defined as the following:

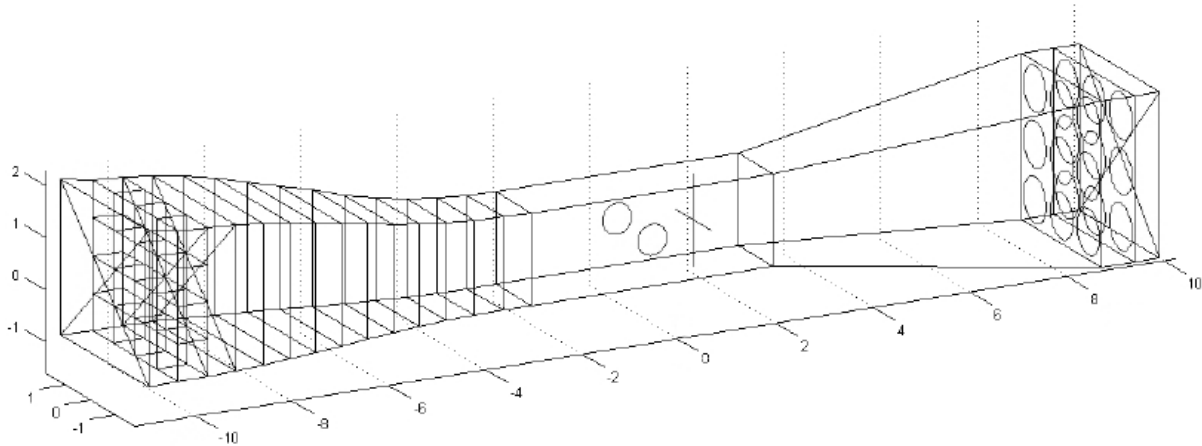$$\chi_{iter,i}^n \cong \frac{(\phi_i^{n+1} - \phi_i^n)}{\lambda_i - 1}$$

(5.13)

Figure 20

Here, n is the number of iterations and λ_i is the eigenvalue of the solution matrix. It could be calculated directly out of the matrix but that is rather time consuming. A fast approximation is given in the following:

$$\lambda_i \cong \frac{\left\| \phi_i^{n+1} - \phi_i^n \right\|}{\left\| \phi_i^n - \phi_i^{n-1} \right\|}$$

(5.14)

The uncertainty in iteration convergence can then be estimated:

$$\Xi_{iter} \cong \frac{\left\| \chi_{iter,i}^n \right\|}{\lambda_{ave} - 1}$$

(5.15)

In the following investigation a solution can be regarded as converged if both the iteration error and the uncertainty in iteration convergence have fallen well below 1% for at least 100 iterations. The graphs for all three cases and the mesh dependency study are presented in Appendix C.

Further, all three calculations (clean wing, raked wingtip and winglet) can be found on the attached CD.

6.   Wind tunnel investigations

6.1.   The wind tunnel

All wind tunnel investigations are carried out at the University of Seville, Spain, at the department of aerospace. The wind tunnel is an open, low speed wind tunnel and its maximum velocity is 28 m/s. Its test section is 1.4m x 1.8m x 5m (w x h x l). A schematic drawing is given in Figure 20. The test section is equipped with two turn tables on each side wall for rotation. Behind the turn tables is a traverse movable in x, y, z direction. Both the turn tables and the traverse are powered by step motors to give them high accuracy. The traverse has an error of ±0.25mm and the turn table of ±0.1°. The free stream velocity is measured using a pitot tube which has an integrated temperature

sensor. There is a 5 hole pressure probe, mountable on the traverse, and three hot wire anemometers (1, 2 and 3 wires) to obtain pressure and velocity information in the wind tunnel. Furthermore there is a balance to obtain the aerodynamic forces. 128 pressure tubes can be connected at the same time to the digital manometer "SYSTEM 8400" from Pressure System Inc. to measure the pressure, 63 of which are used to measure the static pressure on the wing surface. The corresponding data is stored and evaluated in MATLAB. The results are exported as a *.mat file which then can be used for further evaluation.

The wind tunnel is powered by 9 fans which suck ambient air from outside the building into the tunnel. A honeycomb is installed right after the entrance of the tunnel in order to reduce the turbulence level which is below 1%. Due to the fact of using ambient air the wind tunnel can't be used during rainy weather. The ambient has a slight influence on the free stream velocity. It is not possible to hold it at a steady level due to gusts and wind outside the building so there is a slight variation in the free stream velocity during the investigations. In order to get comparable results (e.g. the lift and induced drag coefficient where the free stream velocity appears), the mean of all free stream velocity data points is calculated and used.

6.2.   Measuring the lift coefficient

As described in the previous section, the lift coefficient is measured using the static pressure ports on the wing. In order to gain as much pressure information as possible, only the upper surface of the wing is equipped with pressure ports. This can be done since it is a symmetrical wing. As long as the wingtip devices are as well symmetrical such as the wing extension and the raked wingtip this does not cause any problems but for the winglet it does due to its unsymmetrical nature. In order to obtain the pressure information for the upper and lower surface, two winglets have to be build (normal / mirrored) for measuring the pressure on the surface. With the pressure information available the Cp value is calculated as:

$$C_p = \frac{p - p_\infty}{\frac{1}{2}\rho U_\infty^2} \tag{6.1}$$

The local lift coefficient c_L can be calculated directly from the C_p value as:

$$c_L = \frac{1}{c}\int_0^c \left(C_p^l - C_p^u\right) dx \tag{6.2}$$

This c_L value can be obtained at each row of pressure ports. Their position and amount of pressure ports are given in Table 9:

Name	Number of pressure ports	Position
Row 1	10	$0.14 \cdot c$
Row 2	10	$0.25 \cdot c$
Row 3	10	$0.36 \cdot c$
Row 4	10	$0.46 \cdot c$
Row 5	8	$0.59 \cdot c$
Row 6	8	$0.74 \cdot c$
Row 7	7	$0.89 \cdot c$

Table 9

In order to calculated the overall lift coefficient, i.e C_L from c_L, the local lift coefficient has to be integrated over the half span of the wing:

$$C_L = \frac{2}{b} \int_{0}^{b/2} c_L dy \qquad (6.3)$$

The problem is that there is no local lift coefficient available at the boundary of integration i.e at y = 0 and y = b/2. For y =b/2 the lift coefficient has to be zero. However, the lift coefficient for y = 0 (wing root) must be extrapolated from the other lift coefficients. This is done by:

$$c_{L.y=0} = \left\{ \left[\frac{c_{L,row\ 2} - c_{L,row\ 1}}{0.25 \cdot c - 0.14 \cdot c} \right] (0.00 \cdot c - 0.14 \cdot c) \right\} - c_{L,row\ 1}$$
$$= \left\{ \left[\frac{c_{L,row\ 2} - c_{L,row\ 1}}{0.11 \cdot c} \right] (0.14 \cdot c) \right\} - c_{L,row\ 1} \qquad (6.4)$$

It is more convenient to evaluate (6.2) and (6.3) in one single integral as:

$$C_L = \frac{2}{S} \iint_{S} \left(C_p^l - C_p^u \right) dx dy \qquad (6.5)$$

This is the standard procedure to obtain the lift coefficient a different approach will be presented in 7.4.4 which is a side product of calculating the induced drag coefficient.

It has to be noted that the lift coefficient can also be calculated directly using the lift force obtained from a balance. However, due to the wind tunnel geometry (wing has to be mounted at the side wall) and the heavy wing, the existing balance at the wind tunnel could not be used due to the high bending moment that the wing produces.

Figure 21

7.3   Influencing factors on the results

When it comes to measure flow properties in a wind tunnel there will always be some factors that will alter the results. There are two main factors which influence the results.

The first one is the wind tunnel itself. It is not possible to achieve a perfectly aligned, parallel flow through the test section. Due to its geometry there always will be some degree of crossflow. A picture of the test section with the wing attached to the wind tunnel wall can be seen in Figure 21. This also points out further problems related to the geometry. The first one is the wing. It is mounted on a round block of wood which aim it is to mount the wing to the turn table. The presence of the block will produce a crossflow pointing towards the wingtip near the wingroot. The second problem relating to the geometry is the traverse right behind the wing. Its vicinity affects the flow directly behind the wing. It can be moved a certain distance away so it is not directly behind the wing but then the probe which is mounted to the traverse has to be mounted with a relatively long cantilever arm. This will cause vibration and thus inaccurate results. The effect of the traverse on the behavior of the crossflow has been investigated beforehand and can be seen in Figure 22. Here the crossflow is measured in a region where a preliminary investigation showed a crossflow pointed in the direction of the wingtip but the fluent results a crossflow in the direction of the wingroot. Since the traverse is not the only factor which influence the crossflow behavior, no change in the preceding sign could be noted. However, the crossflow changes into the right direction when the traverse is moved backwards. The distance of the traverse moving backwards has been made dimensionless with the mean aerodynamic chord (c_{MAC} = 0.34m). A position for the traverse has been chosen as far as possible behind the wing where the vibration could still be kept at a minimum level.
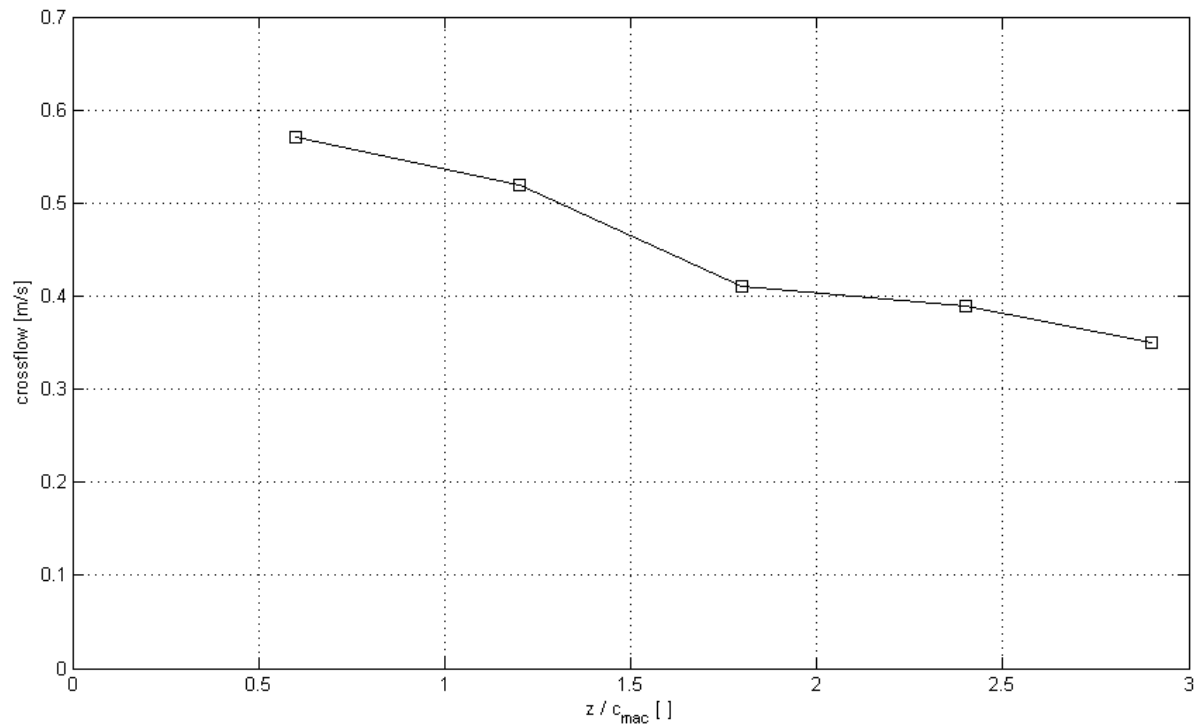
Figure 22

The second factor to influence the result is the probe itself. For the current investigation a 5 hole probe has been used to determine the crossflow at the trailing edge. It is not possible to mount the probe in a way that it is perfectly aligned with the free stream. In order to obtain the real value for the crossflow, the traverse was moved into the middle of the wind tunnel with no wing attached to the wall and then a measurement of the free stream has been done. In theory, if everything would have been mounted perfectly, there would be no crossflow. However, a small amount of crossflow was measured (less than 5%). This amount is taken as an offset value, which later is to be subtracted from the actual crossflow results.

6.4.   Measuring the induced drag coefficient

7.4.1   The five hole pressure probe

The five hole pressure probe measures the pressure in a plus formation in order to obtain the direction and magnitude of the flow. The plus formation is necessary to measure in all three coordinate directions.

There are two ways of operating the probe namely the calibrated and non-calibrated method. Calibrated means in this context that the probe has to be aligned with the free stream. Hence, with no obstacles in its way the crossflow and the down wash are zero. As discussed in the previous section, this is hardly achievable. That is why the offset value has to be subtracted from the results.

The second way of operating the five hole pressure probe is the non-calibrated method. Here, the probe is located to the position where measurements should be taken. Now the probe rotates into a position where it does not measure any crossflow or down wash anymore. The angle of the probe with respect to the free stream is then taken to calculated the crossflow and down wash angle and

the velocity can be determined. A traverse with 5 degrees of freedom is needed to perform that analysis.

The first method is being used since the traverse used for the investigation offer only 3 degrees of freedom.

In the next three section there will be a discussion of three different approaches to obtain the induced drag using the pressure probe. Method one is the Trefftz-plane analyze and is very popular to obtain the induced drag. For it to work it needs the crossflow and the down wash velocity. Method two and three are less popular but need just the crossflow and are therefore interesting in order to reduce testing time. They will be discussed in great detail in the following.

7.4.2   Method 1: Trefftz-plane analyze

As outlined before, the Trefftz-plane analyze is the most popular way of obtaining the induced drag. It can be derived from the momentum equation given in (5.2). A profound derivation can be found in various literatures. The formula for the induced drag is:

$$D_i = \frac{1}{2}\rho \iint\limits_{S_T} (v^2 + w^2)dS \tag{6.6}$$

The induced drag is made dimensionless by:

$$C_{Di} = \frac{D_i}{\frac{1}{2}\rho U_\infty^2 S} \tag{6.7}$$

Here, S_T is the Trefftz-plane far behind the wing. Equation (6.6) states that the induced drag is directly related to the crossflow and down wash. As discussed in chapter 2.2 the air that passes a wing will create a vortex due to the pressure difference at the wings upper and lower surface. This vortex is then measured in terms of crossflow and down wash velocity at the Trefftz-plane to obtain the induced drag. In other words, the induced drag is the kinetic energy which is transferred into the crossflow.

Although the Trefftz-plane is the common way of obtaining the induced drag it could not be achieved in the present investigation due to the time penalty of the traverse. It moves too slowly in order to obtain a sufficient resolution of data points behind the wing. Furthermore the traverse could not be moved very far away from the wing which still had an influence on the crossflow as discussed before. That makes it not suitable for the present investigation however it is a very fast and good way to obtain the induced drag in FLUENT.

In order to get the induced drag a different approach has to be done which will be discussed below.

7.4.3   Method 2: Crossflow I

The first approach to obtain the induced drag from just the crossflow is derived from Prandtl's lifting-line theory. From that theory the induced drag coefficient in general can be expressed as:

$$C_{Di} = \frac{1}{2\pi S U_\infty^2} \int\limits_{-b/2}^{b/2} \Gamma(y)dy \int\limits_{-b/2}^{b/2} \frac{\frac{d\Gamma(y)}{dy}}{y_0 - y} dy \qquad (6.8)$$

The only unknown variable in (6.8) is the circulation $\Gamma(y)$. It can be obtained from:

$$v^+(y) = \frac{1}{2}\frac{d\Gamma(y)}{dy} \qquad (6.9)$$

Substituting (6.9) into (6.8) it becomes:

$$C_{Di} = \frac{1}{\pi S U_\infty^2} \int\limits_{-b/2}^{b/2} \Gamma(y)dy \int\limits_{-b/2}^{b/2} \frac{v^+(y)}{y_0 - y} dy \qquad (6.10)$$

Here, v^+ resembles the crossflow. The question arises where to measure that crossflow. It is a reasonable choice to choose the trailing edge as a reference for the measurements since the vortex will have started to build up when it reaches this region however it is still not clear where exactly the maximum crossflow is to be expected which is crucial to get the right results. In order to investigate the impact of the position on the crossflow behavior the velocity was measured at various position in front of the trailing edge (i.e. over the wing surface) and behind the trailing edge showing no significant change in the velocity. Furthermore, the velocity profiles at some locations along the span where taken moving upwards behind the trailing edge to see the change in the crossflow over height. It could be concluded that the crossflow changes so drastically that the maximum crossflow value has to be determined at each position individually. It is not possible to take measurements at some points and connect those points linearly. The maximum crossflow value changes, especially at the wingtip where the greatest values are to be expected. Keeping that in mind, there has to be always two measurements, one, to obtain the maximum crossflow value and its corresponding position by sweeping through a plane behind the wing and the second, to obtain the value for the crossflow at that exact location by using a longer, stationary measurement. It can be said that it is not always clear where the maximum value for the crossflow is, most of the times, especially near the wing root, the crossflow has a evenly distributed velocity profile over its height. Moving further to the wingtip the velocity profiles show sometimes two, hardy distinguishable maximums due to their evenly distributed nature. It is not until the measurements are taken in the vicinity of the wingtip that a clear maximum arises. The velocity profiles can be easily reconstructed in MATLAB from the raw data provided in Appendix A.
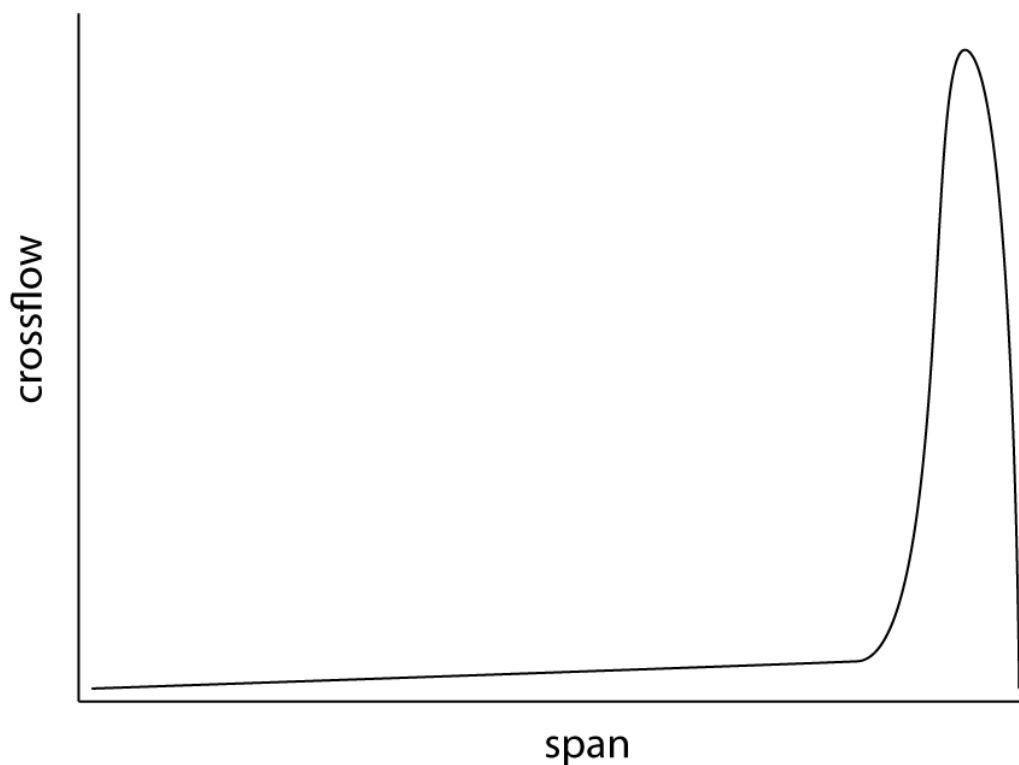
This approach seems straight forward but the problematic nature lies in the details and it can be seen by looking at Figure 23. It shows a schematic sketch of the crossflow along the half span of a wing that could be expected for a wing without any wingtip modification.

Right in the vicinity of the wingtip there is a huge and sudden change in the crossflow. To capture that change and to resolve the crossflow profile with good accuracy a vast numbers of data points have to be taken in that region. Turning back to (6.10) we see for the last integrant that we would expect a high crossflow but we divide it by a very small number due to the fine measurement resolution. y_0 is a fixed location on the wing while y is a variable that runs across the wing. As y approaches y_0 and its value zero i.e. $|y_0 - y| \rightarrow 0$ (for an infinite resolution of y), the actual value of crossflow at that position is very large at the wingtip so that a very great value is divided by a value near to zero. This can be seen in Figure 24. Here, the last integrant is evaluated for all y_0 along the span. As can be seen the magnitude changes in orders over the span and by that making the whole formula instable. The results however are in a region where they are to be expected. The real problem becomes obvious if just one single data point is taken out of the calculation. The results will change, sometimes even in magnitude. That proposes that absolute precision and accuracy is needed for this method to work. This precision and accuracy could not be achieved.

To conclude this section it can be said that formula (6.8) might work in theory but is hardly applicable to practical engineering problems. That being said, a different approach has to be found that can be used. This will be discussed in the next section.
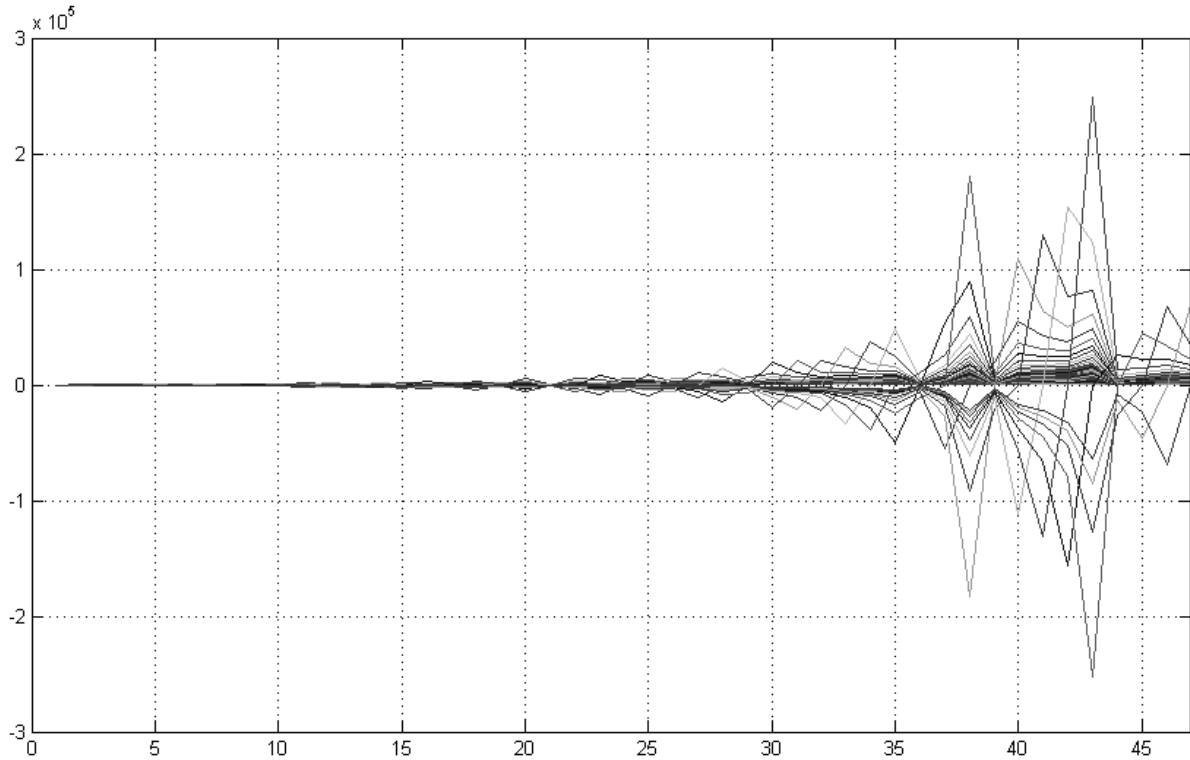
7.4.4   Method 3: Crossflow II

The third and final approach uses a fast fourier transformation to obtain the induced drag. First, the fourier coefficients B_m has to be calculated using:

$$\int_0^{\pi} cos(m\theta) \frac{v^+}{U_{\infty}} d\theta = m \frac{B_m}{2} \frac{\pi}{2} \tag{6.11}$$

Since computational time is no issue a rather great amount of fourier coefficients can be calculated. It can be shown that the results do not change anymore for values of m greater than 50. Therefore m is set to 50.

The induced drag can be calculated as:

$$D_i = \frac{\pi}{8} \rho U_{\infty}^2 b^2 \sum_{m=1}^{\infty} m B_m^2 \tag{6.12}$$

Further, the Lift can be calculated using the first fourier coefficient:

$$L = \frac{\pi}{4} \rho U_{\infty}^2 b^2 B_1 \tag{6.13}$$

Using equation (3.11) and (6.7) the induced drag and lift can be made dimensionless. Using the lift coefficient is a good way of gaining trust in the method, once the lift coefficients are comparable, the induced drag values will be comparable as well.

7.5 Results

The final results obtained in the numerical simulation and in the wind tunnel are presented in Table 10:

	Clean Wing		Raked wingtip		Winglet	
	Experiment	FLUENT	Experiment	FLUENT	Experiment	FLUENT
C_L	0.3972	0.3810	0.4127	0.4070	-[1]	0.3871
C_L FFT	0.3076	0.338	0.3848	0.3881	0.5005	0.0867
C_{Di} FFT	0.0059	0.0066	0.0076	0.0073	0.0107	0.0004
C_{Di} Trefftz-plane	-	0.0046	-	0.0044	-	0.0043

Table 10

Furthermore the charts for the crossflows of each configuration is given in Figure 25 to Figure 27.

The crossflow does compare well for the clean and raked wing configuration while there is a big difference for the winglet at the wingtip which is the crucial and the most important part for calculations. The reason is that the crossflow for the clean and raked wingtip has to be measured only in one dimension. Measuring the crossflow for the winglet means to measure the crossflow in two dimension. Hence, not only the crossflow but also the down wash has to be measured and then
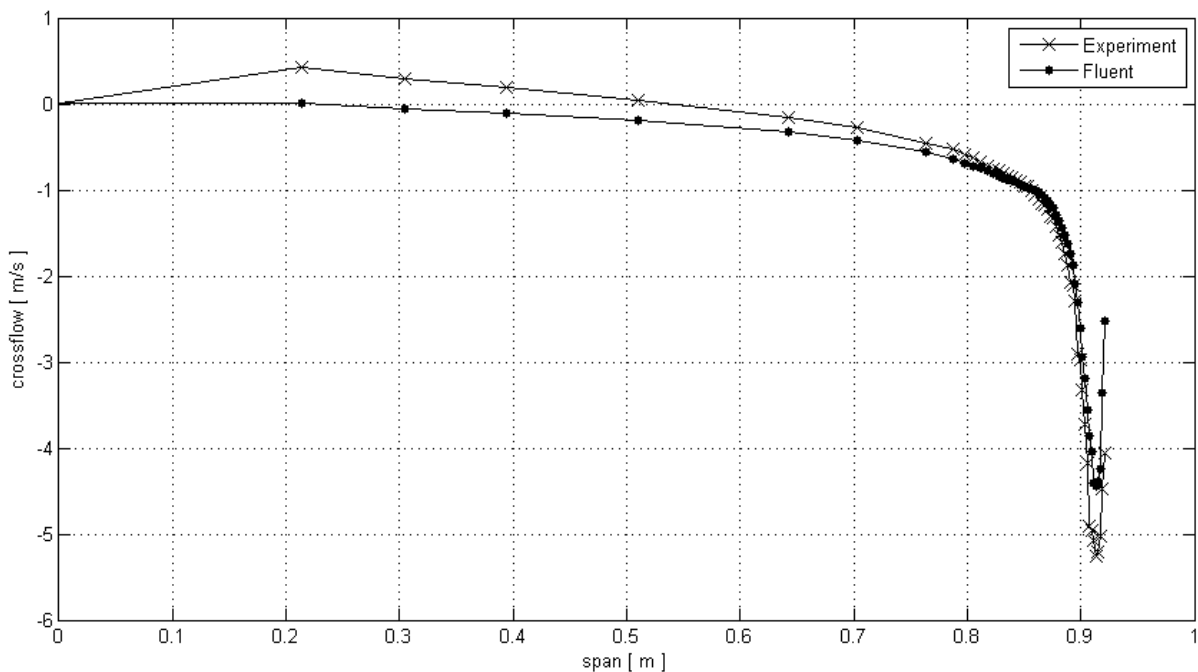

Figure 25

---

[1] Due to a massive problem with the 3D printer at the end of the investigation, the second winglet which is necessary to obtain the static pressure on the lower wing surface could not be printed. Therefore the lift coefficient for the winglet could not be obtained.
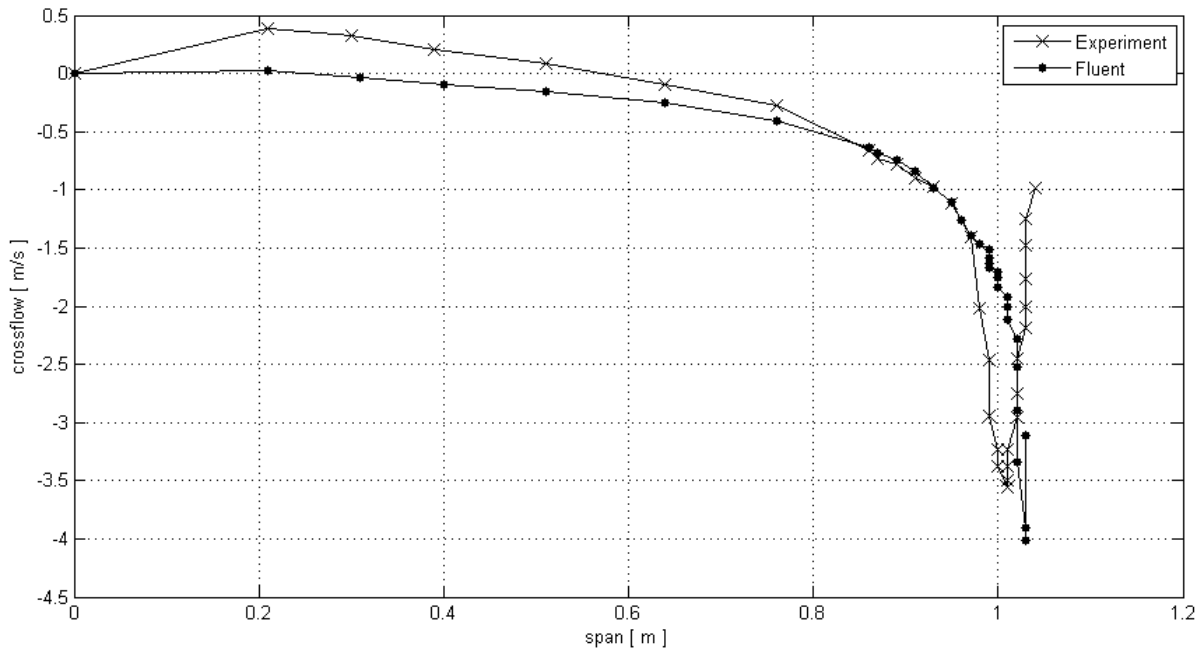
Figure 26
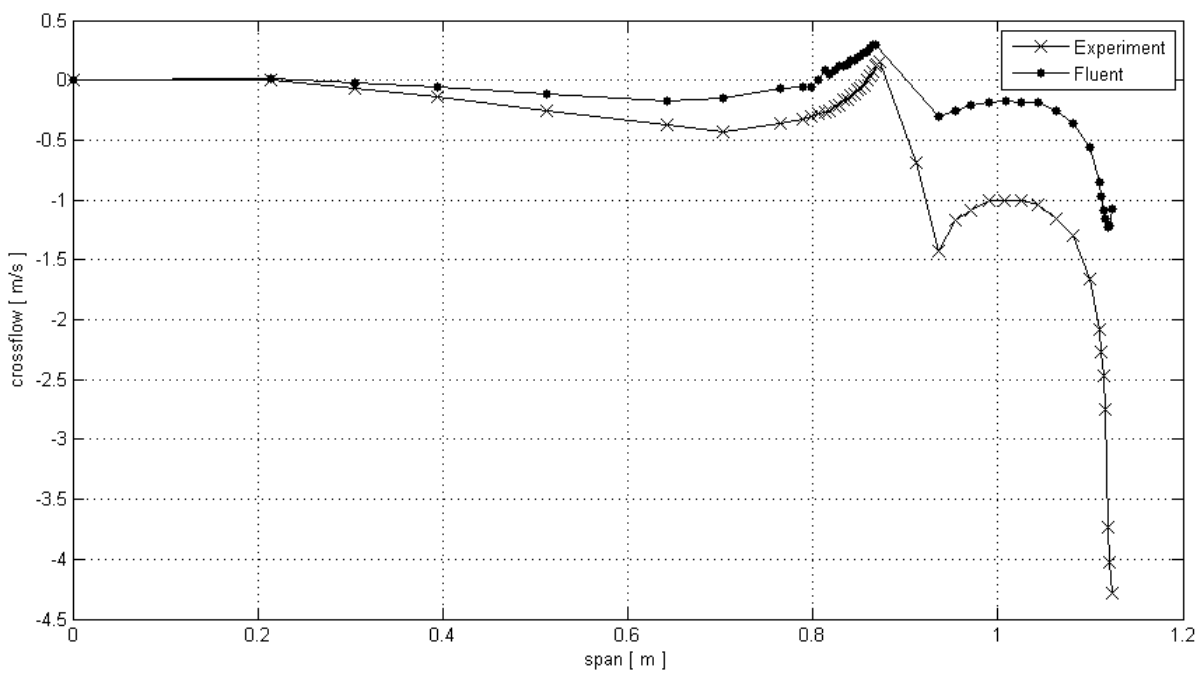
Figure 27

these two values have to be put together. Observing each component, i.e. crossflow and down wash in Figure 28 and Figure 29 it can be seen that the crossflow is captured well, just as before, however the down wash shows a significant difference. A big contributing factor is the wind tunnel itself, no measurements taken in a wind tunnel resembles the reality, there are always errors in the results due to the geometry. Since it is a constant offset which correspond to an angle of 5° this explanation seems plausible.

Figure 28

Turning back to Table 10, the first value, C_L, is obtained by using the static pressure ports on the wing surface. The second value, C_L FFT, is the lift coefficient obtained from the fast fourier transformation (FFT) using equation (6.13) and (3.11). The first value for the induced drag, C_{Di} FFT, is obtained from the fast fourier transformation as well, usin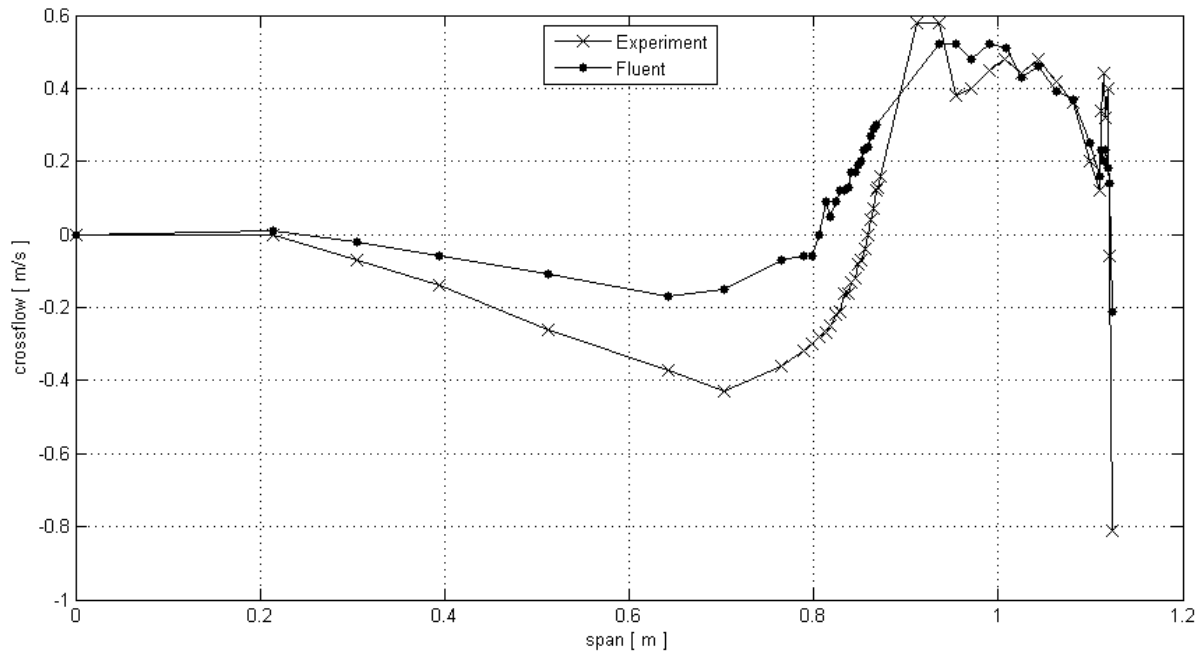g equation (6.12) and (6.7) this time. The last value, the C_{Di} Trefftz-plane, is obtained by using the Trefftz-plane from equation (6.6) and (6.7). As mentioned before it is too time consuming to perform the Trefftz-plane analyze in the experiment. That is the reason why only FLUENT is capable of producing those results.

As can be seen in Figure 25 to Figure 27 the experimentally obtained crossflow differs from the numerical obtained crossflow near the wing root. In order to obtain the values for the fast fourier transformation this behavior had to be compensated by assuming a zero crossflow at this region which is a reasonable assumption. That is necessary since the lift coefficient is calculated by using only the first fourier coefficient. Without the correction the first fourier coefficient would depend on an unrealistically flow behavior and therefore produce unrealistically results.
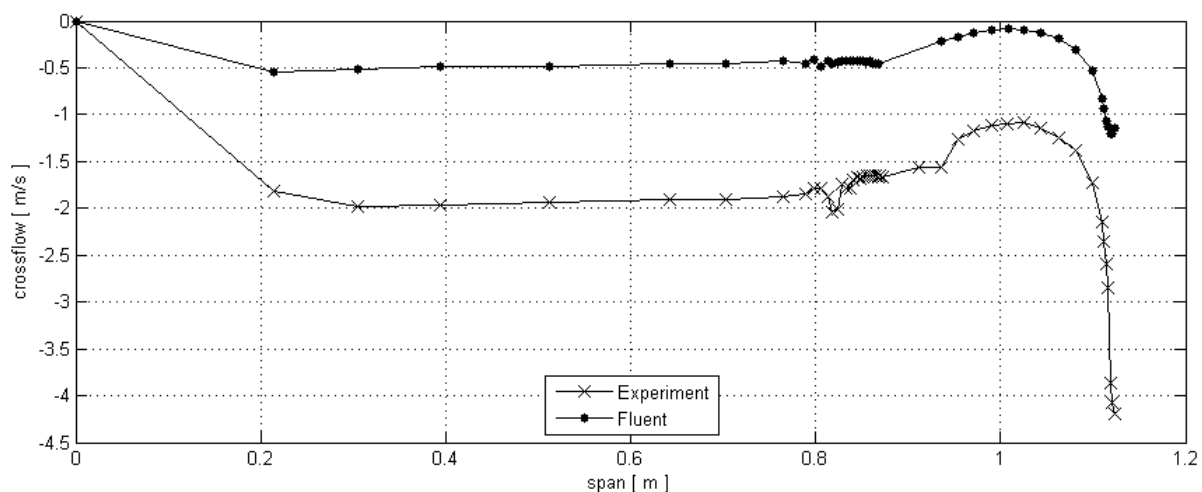

Figure 29

Looking at the results it can be stated that the lift coefficient for the experiment compares well to the values obtained in FLUENT and vice versa. It would have been great to get a value for the winglet which, unfortunately, was not possible. The lift coefficient was calculated as previously in the TORNADO investigation, making them dimensionless by their new span and new wing surface area. For the clean and the raked wing configuration the results calculated for the lift coefficient using the FFT do not differ too much. That is not necessarily self-evident, keeping in mind that the crossflow near the wing root had to be modified. That speaks out for this method as a fairly stable method in comparison to the method introduced in section 7.4.3. There is no source to which the lift coefficient obtained for the winglet can be compared against however when compared to the FLUENT result it shows that it is again in the right region where it should be but probably not as accurate as the lift coefficient obtained from the pressure ports would have been. However, the primary goal of obtaining the lift coefficient with this method was to ensure, that this method works and produces reasonable results. Since the results are fairly well given the experimentally nature of this approach the induced drag coefficient can be obtained and examined.

Again, for the clean and raked wing configuration the induced drag coefficient compares quite well except for the winglet. Looking at Figure 27 this does not surprise since there is a significant difference in the graphs. As pointed out, the down wash is much higher in the wind tunnel than in the free stream. Looking at the same time at the induced drag coefficient obtained in FLUENT using the Trefftz-plane analyze one important fact can be seen: The clean and raked wingtip configuration are within the magnitude and also quite close to the Trefftz-plane values. The induced drag coefficients for the winglet obtained in the fast fourier transformation differ away from the value obtained with the Trefftz-plane analyze. The conclusion is that the measurement of the induced drag coefficients using the fast fourier transformation can be improved by spending more time addressing the problems due to the wind tunnel geometry that have been discussed before. Also, the results for the winglet show that the down wash (in the global coordinate system) at the wingtip has a high influence on the measurement of the induced drag coefficient. Suggestions to overcome this problem will be states in chapter 7.

Furthermore, the induced drag coefficients obtained using the fast fourier transformation state that the clean wing is the best wing configuration followed by the raked wingtip and only then the winglet. This results point out another thing: Although it is possible to measure the induced drag coefficient with this method and even though it is near the value of the Trefftz-plane analyze it does not produce trustworthy results. It is a fairly easy method for one dimensional measurements but becomes fast more complex when two dimensional measurements such as for the winglet configuration have to be taken. In contrast, the Trefftz-plane analyze does not depend on the geometry and therefore obtains the induced drag value always in the same manner making the results comparable and apparently more trustworthy. Looking at those results more closely it becomes clear that they are the only results that can really be trusted. As expected, the clean wing configuration produces still the most induced drag while the raked wingtip is able to reduce it. The winglet shows the most reduction in induced drag but only just.

Another way is to look at the maximum crossflow value obtained experimentally. The clean wing reaches a value of $v_{max}^+ = 5.2 \; {}^m/_S$, the raked wingtip of $v_{max}^+ = 3.6 \; {}^m/_S$ and the winglet of $v_{max}^+ = 4.3 \; {}^m/_S$. The crossflow is reduced for the wingtip modifications. The raked wingtip has the smallest value but it seems that has a larger region of high crossflow values while the winglet only

peaks at one point having a small region of high crossflow values. That is not a very conclusive way of judging the intensity of the vortex behind the wing but gives an idea of what can be expected. A better way would be to study the vortex behind the wing at a given distance most preferable at the Trefftz-plane. Such a study for a similar experimentally setup can be found in Zingel [20].

To conclude this section, the results should be compared against the TORNADO results as well. Doing that it becomes apparent that there is a significant difference between the experimental / FLUENT and the TORNADO results. Those deviation are such high that they should be addressed in its own section.

7.6   Revision: TORNADO results

Looking at Table 10 and comparing it against Table 3, Table 4 and Table 5 it is obvious that there is a great difference for the TORNADO results compared against the experimental and numerical results. To find the root causes of the problem changes have been done to the setup of the cases in TORNADO trying to find the problem and eliminating it. One of the first things was to change the mesh type. There are 7 different approaches to mesh the wing in TORNADO such as linear, cosine meshing and combination of them. The complete list, taken directly from TORNADO is:

[1] Linear

[2] Spanwise half-cosine

[3] Spanwise half-cosine, chordwise cosine

[5] Spanwise cosine

[6] Chordwise cosine

[7] 3rd order centerpacking. (Not for wings)

Changing the mesh and the numbers of panel however did not affect the results too much. Some changes were noted but they were only marginal. Since that did not affect the problems very much the wing was rebuilt to assure no modeling errors were made but even that did not solve the problem. In a final attempt the wing was mirrored at the wing root. For all the other investigation done prior to this one the wing was modeled as it would be in the wind tunnel i.e. the wing was just modeled for one side going from 0 to b/2. This was done in order to achieve consistency for the result since not only the wind tunnel but also the FLUENT investigation investigate only one side of the wing.

The normal workflow in TORNADO is that just one part of the wing is created and then TORNADO asks explicitly if the wing should be mirrored or if it should be investigated just as it is. This workflow suggests that both calculations are doable in TORNADO and in order to reduce computational time the non symmetrical setup seems to be the better choice. However, as it turns out, TORNADO produces two complete different results for the mirrored and non-mirrored case. Furthermore, beside the master-thesis [13] published by the author of TORNADO (which only states the mathematical background of the vortex-lattice code) there is no manual or other source of

information that warns about this and potentially other problems. However, the vast amount of data that was examined during the first iteration process suggested that the results were reasonable since the bending moment increased from the wingtip to the wing root and the local lift coefficient showed a curved distribution over the span just as it would be expected. No concerns were raised after the first results were obtained. After the FLUENT results were accessible first deviations were noted but to judge whether the FLUENT or TORNADO results were flawed we waited until the experimentally results were available. Only then it became obvious that something was wrong with the TORNADO results which gave the need for a revision.

With the error found to solve the problems, all calculations are done again in TORNADO. The results are shown in Table 11:

	C_L	C_B	C_{Di}
clean wing	0.3599	0.203	0.0068
raked wingtip	0.3703	0.191	0.0066
winglet NACA 2408	0.3379	0.184	0.0067
winglet PSU	0.3423	0.188	0.0067
winglet NACA 0413	0.3362	0.185	0.0064
winglet whitecomb	0.3288	0.173	0.0063

Table 11

Now the values compare much better to the experimentally and numerically results obtained for the lift coefficient. The induced drag coefficients are obtained using the integrated Trefftz-plane analysis within TORNADO. However, in TORNADO, the Trefftz-plane analyze is still an "experimental" stage. What that means can only be guessed, as mentioned before there is no manual or other sources that can be consulted for information on that. Hence, those results should be regarded with care.

Looking at Table 11 it can be seen that the clean wing configuration without any wingtip device produces the highest root bending moment coefficient and the highest induced drag coefficient. The raked wingtip as well as the four winglet designs are all able to reduce the root bending moment and the induced drag. However, now the winglet design suggested by whitcomb seems to be the best choice for the winglet design since it reduces the induced drag the most. It even produces a lower bending moment at the wing root than the raked wingtip. This comes with some surprises since the raked wingtip is said to reduce the bending moment more than the winglet. However, not only does the raked wingtip reduces the root bending moment it also reduces the twisting moment of the wing which is not calculated in TORNADO. This means that no clear and definite answer can be given whether the raked wingtip reduces the loads on the root more than the winglet.

The trend that the induced drag values from the FLUENT results tell is captured well. The clean wing without any wingtip device produces as expected the most induced drag followed by the raked wingtip. The best way to reduce the induced drag from the aerodynamic point of view is still the winglet.

Unfortunately for the present investigation, that error was fixed at such a late point in the investigation that the winglet geometry could not be changed anymore. That means that the results for the winglet obtained in the wind tunnel could have been even better than stated in Table 10.

7.   Conclusion

In the following investigation the influence of different wingtip devices, namely the raked wingtip and the winglet, was investigated at the university of Seville using wind tunnel experiments and numerical simulations in FLUENT. The optimum design for the winglet was found iteratively while the raked wingtip design is heavily based on boundary conditions that makes the design process straight forward. The main goal was to see with design is able to reduce the induced drag the most.

It has been shown that a wing without any wingtip devices produces the most induced drag. Both the raked wingtip and winglet design are able to reduce the induced drag while the winglet is still the best choice to reduce the induced drag the most under the aerodynamic point of views. The final influence of the raked wingtip in terms of the reduction in loads at the wing root could not be captured. Here, the vortex-lattice code TORNADO, which was used to obtain the preliminary design, reaches its limits. In order to investigate this effect for a real setup, the easiest way is to measure the forces and moments on the wing with and without the raked wingtip. Furthermore a fluid-structure interaction (FSI) simulation could be done in FLUENT to couple the aerodynamic forces with the structure of the wing. This effect for itself is worth an investigation on its own and could not be investigated to its full extend. The effect of the raked wingtip on the structural part of the wing is quite significant. Studying the literature it becomes evident that the raked wingtip is designed to not only reduce the induced drag by its aerodynamic shape but also to reduce the structural loads in order to reduce the structural mass of the aircraft.

As has been shown using the Trefftz-plane analyze, the winglet outplays the raked wingtip configuration marginally. Also, the Trefftz-plane analyze has shown its stability for obtaining the induced drag hence proving why it is the standard for obtaining the induced drag.

Furthermore two different approaches were presented to obtain the induced drag. The first one presented was too instable to produce useable results. The second one struggled with the wind tunnel geometry itself. To overcome the problem of the wall, a new, scaled wing should be constructed or printed, this time being symmetrical going from –b/2 to b/2 and placed in the middle of the tunnel. In this way there should be a real zero crossflow in the middle but also, since the design is symmetrically, the vortices at each wingtip will influence the crossflow behavior such as they would do on a real wing. Therefore, the unrealistically crossflow that was measured in the present investigation can be eliminated. It would be very useful to measure the aerodynamic forces as well for future investigations. If new investigations are done in the present wind tunnel, they should be done with smaller, scaled models in order to use the balance.

It has been discussed that an inward canted winglet reduces the wing root bending moment as well. In the phase of preliminary sizing it was observed that the induced drag increases for that configuration. It may be possible to reduce the bending moment with an inward canted winglet by the same magnitude as the raked wingtip but still gain a greater reduction in the induced drag.

As was mentioned early, there is a new design trend to combine the raked wingtip and the winglet configuration. For further investigations it would be very helpful to have a combined wingtip to investigate its impact on the induced drag.

8.   References

[1]   Richard T. Whitcomb (1976)
         A design approach and selected wind-tunnel results at high subsonic speeds for wing-tip
         mounted winglets
         NASA TN D-8260

[2]   Peter K. C. Rudolph (1991)
         High taper wingtip extension
         US patent, patent number: 5,039,032

[3]   Larry L. Herrick, Byram Bays-Muchmore, Michael S. Hoffman, L. LeGrand, Steven S. Ogg,
         Bernard P. Paul, Jr., Kenneth D. Visser, Stepehn L. Wells (2003)
         Blunt-leading-edge raked wingtips
         US patent, patent number: 6,089,502

[4]   Louis B. Gratzer (1994)
         Blended winglet
         US patent, patent number: 5,348,253

[5]   Mark D. Maughmer (year unknown)
         About Winglets

[6]   Mark D. Maughmer, Timonthy S. Swan, Steven M. Willits (2001)
         The design and testing of a winglet airfoil for low-speed aircraft
         19th applied aerodynamics conferences, CA, June 11-14
         AAIA Paper 2001-2478

[7]   Mark. D. Maughmer (2001)
         The design of winglets for high-performance sailplanes
         AAIA Paper 2001-2406

[8]   Fritz Dubs (1954)
         Aerodynamik der reinen Unterschallströmung
         Birkhäuser

[9]   J. E. Hackett (year unknown)
         Vortex drag reduction by aft-mounted diffusing vanes
         Lockheed-Georgia Company
         ICAS-80-13.4

[10]   Robert J. McGhee, William D. Beasley (1976)
         Effects of thickness on the aerodynamic characteristics of an initial low-speed family of
         airfoils for general aviation applications
         NASA Technical Document (NASA TM X-72843)

[11]   Richard J. Margason, John E. Lamar (1971)
         Vortex-Lattice fortran program for estimating subsonic aerodynamic characteristics of
         complex planforms
         NASA TN D-6142

[12]   Joseph Katz, Allen Plotkin (2001)
         Low-Speed Aerodynamics
         Cambridge University Press

[13]   Tomas Melin (2000)
         A Vortex Lattice MATLAB Implementation for Linear Aerodynamic Wing Applications
         Master thesis / The Royal Institute of Technology

[14]   Daniel Schiktanz
         Untersuchungen von Tragflügelumströmungen mittels TORNADO
         Project / HAW-Hamburg

[15]   Juan Manuel Gonzalés Cantero (2011)
         Alas en régimen subsonic
         Aerodinámica II, 4o Ingenierá aeronáutica

[16]   Ira H. Abbott, A. E. Von Doenhoff (1960)
         Theory of Wing Sections: Including a Summary of Airfoil Data
         Dover Pubn Inc.

[17]   Robert J. McGhee, William D. Beasley, Dan M. Somers (1975)
         Low-speed aerodynamic characteristics of a 13-percent-thick airfoil section designed for
         general aviation applications.
         NASA TM X-72697

[18]   Ismail B. Celik, Urmila Ghia, Patrick J. Roache, Christopher J. Freitas,
         Hugh Coleman, Peter E. Raad (2008)
         Procedure for estimation and reporting of discretization error in CFD applications
         Morgantown, West Virginia University,
         Mechanical and Aerospace Engineering Department
         Journal of Fluids Engineering, Vol. 130

[19]   P. J. Roache (1994)
         Perspective: A method for uniform reporting of grid refinements studies
         Albuquerque, Ecodynamics Research Associates Inc.
         Journal of Fluids Engineering, Vol. 116, p. 405-413

[20]   Hartmut Zingel (1998)
         Der Flügelspitzenwirbel und seine Beeinflussung durch den Flügelrandbogen
         Hamburg, Hamburg university of applied science
         Mobiles 24, p. 52-55

I.   Appendix A

The following structure is given on the CD with explanation below:

Folder: 3D systems

- Contains the introducing video of the 3D printer

Folder: Bachelor thesis

- Contains this thesis as a PDF file

Folder: CATIA

- Contains all relevant CATIA constructions (compatible with CATIA V5 R20 or higher versions)

Folder: Excel Files

- Contains all relevant Excel files that have been created during this thesis

Folder: FLUENT

- Contains the casa and data file in a zipped format (in order to fit on the CD)
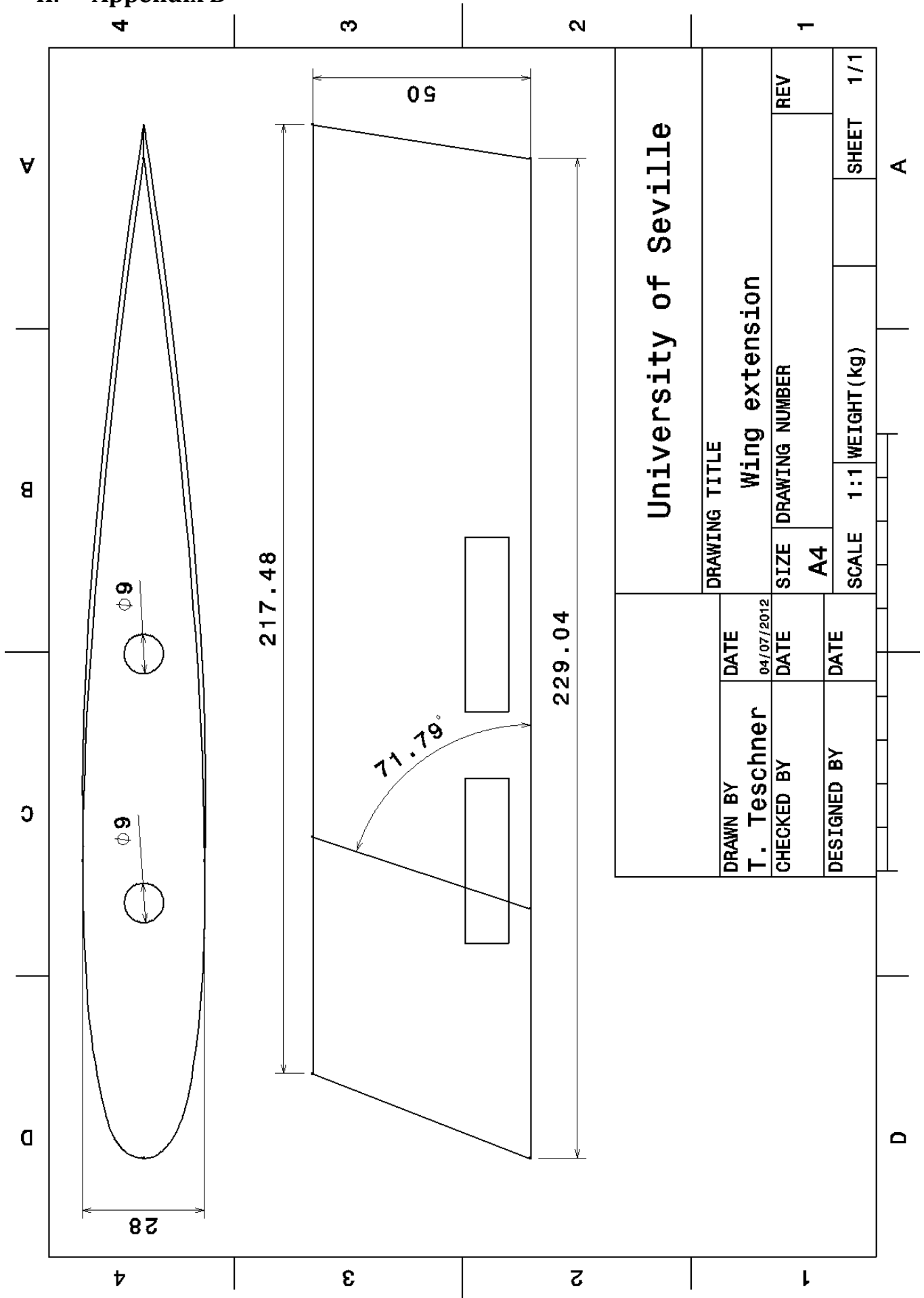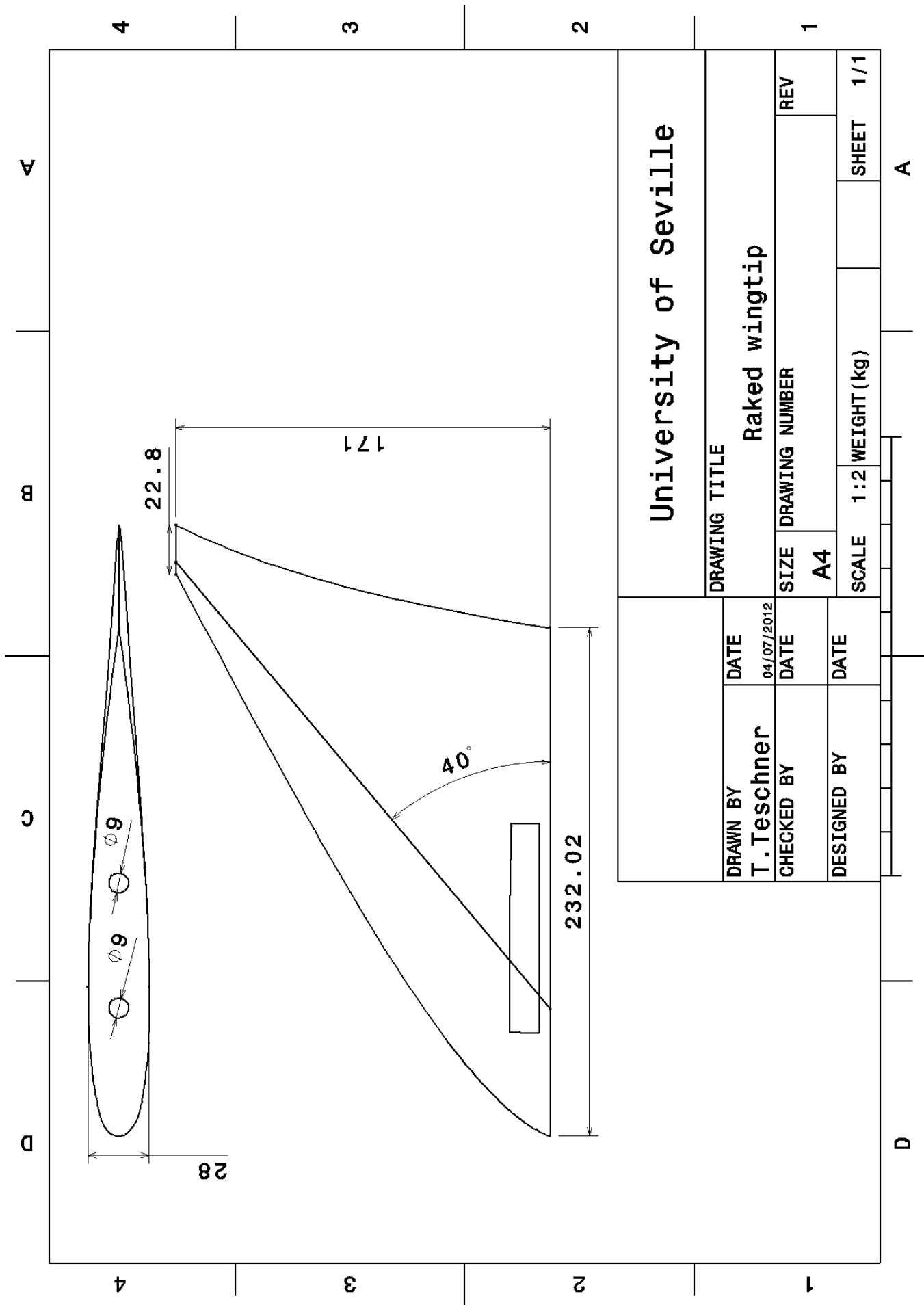
Folder: MATLAB

- Contains all relevant MATLAB files that have been created during this thesis
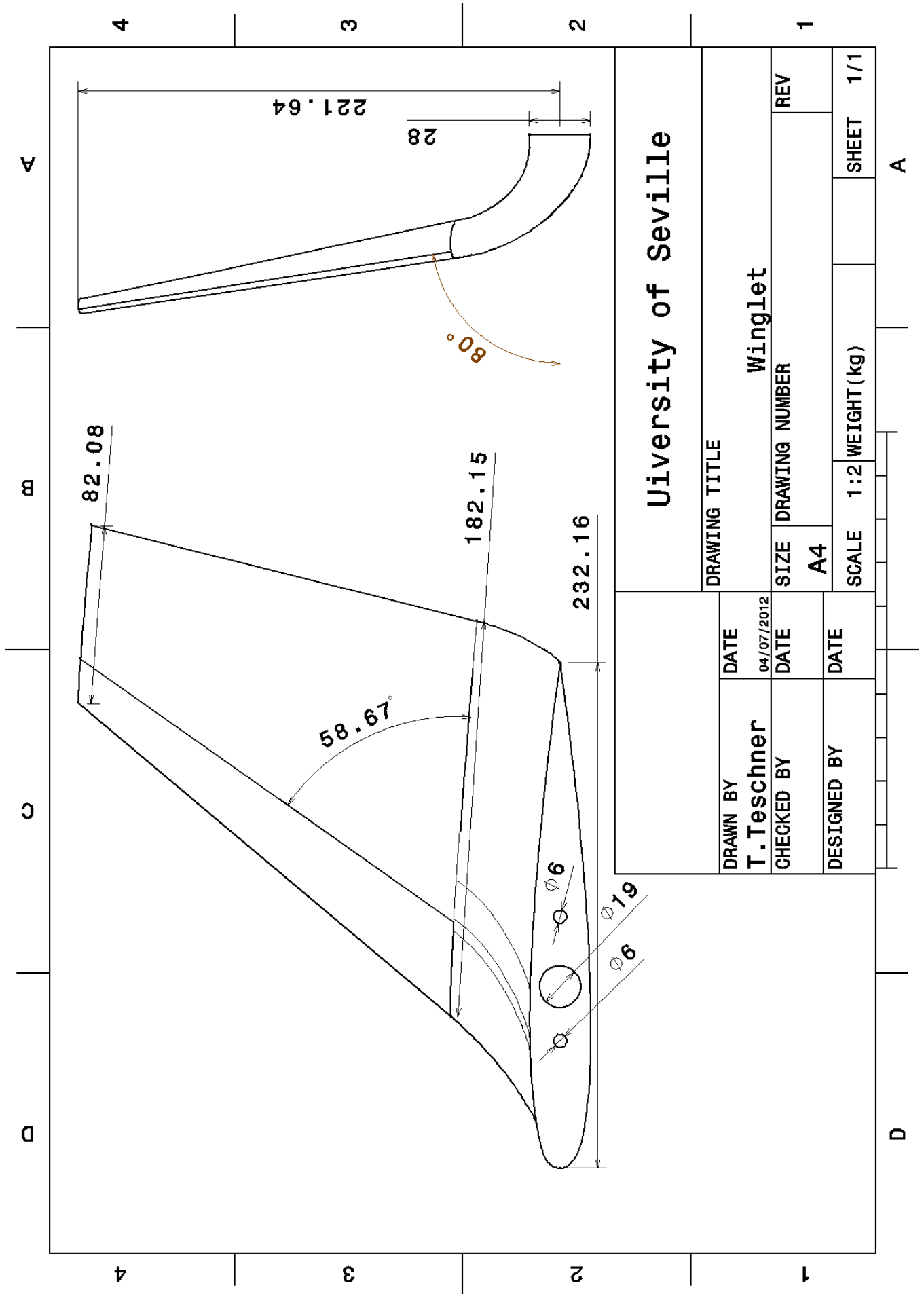
Folder: Wind tunnel raw data

- Contains all the raw data information as well as the lift coefficient evaluation (missing for the winglet)

II. Appendix B

University of Seville

Raked wingtip

DRAWING TITLE			
DRAWN BY	DATE		
T.Teschner	04/07/2012		
CHECKED BY	DATE	SIZE	DRAWING NUMBER
		A4	
DESIGNED BY	DATE	SCALE 1:2	WEIGHT(kg)

REV

SHEET 1/1

171

22.8

40°

232.02

Ø9

Ø9

28

Uiversity of Seville

DRAWING TITLE		Winglet		
DRAWN BY	DATE			REV
T.Teschner	04/07/2012			
CHECKED BY	DATE	SIZE	DRAWING NUMBER	
		A4		
DESIGNED BY	DATE	SCALE	1:2	WEIGHT (kg)
				SHEET 1/1

221.64
28
80°
82.08
182.15
232.16
58.67°
Ø6
Ø19
Ø6

III.   Appendix C

Table 12 gives the details for the three different meshes that are being used for the mesh dependency studies. The overall volume is 7137.896 m². The raked wingtip configuration has been used for conducting the study.

	Coarse mesh	Medium mesh	Fine mesh
Cells	1 044 739	1 775 076	3 200 715
C_L	0.39982	0.40144	0.40197

Table 12

The results for equation (5.8) to (5.11) are given in Table 13:

ϕ_{ext}^{32}	0.4022
ϕ_{ext}^{21}	0.4022
e_a^{32}	0.4035
e_a^{21}	0.1319
e_{ext}^{32}	0.1810
e_{ext}^{21}	0.0492
GCI_{fine}^{32}	0.2266
GCI_{fine}^{21}	0.0615

Table 13

What Table 13 basically states is that the value of C_L will converge for an infinite mesh size i.e.:

$$\lim_{mesh \to \infty} C_L = 0.4022 \qquad (III.1)$$

There is a second, very famous extrapolation method for obtaining the extrapolated value of ϕ, namely the "Richardson extrapolation", which in nature is less complex yet less accurate. The extra effort of the method used by Celik gives stable results as can be seen.

The absolute and the extrapolated error are below 1% which indicates that the value of C_L does not change very much from mesh to mesh size.

Finally the grid convergence index can be calculated. As can be seen, even this value is below 1%. This states that the medium grid is sufficient for further investigation. Even the coarse grid could be used but a coarser grid has to be produce and taken into account for the mesh dependency study in order to be sure. Still, the fine mesh produces relatively quick results (calculation time within 24 hours). Therefore the fine mesh has been used for further investigations.

The iteration error and uncertainty in iteration convergence for the last 100 iteration of each calculation (clean wing, raked wingtip and winglet) are given in Figure 30 to Figure 32.
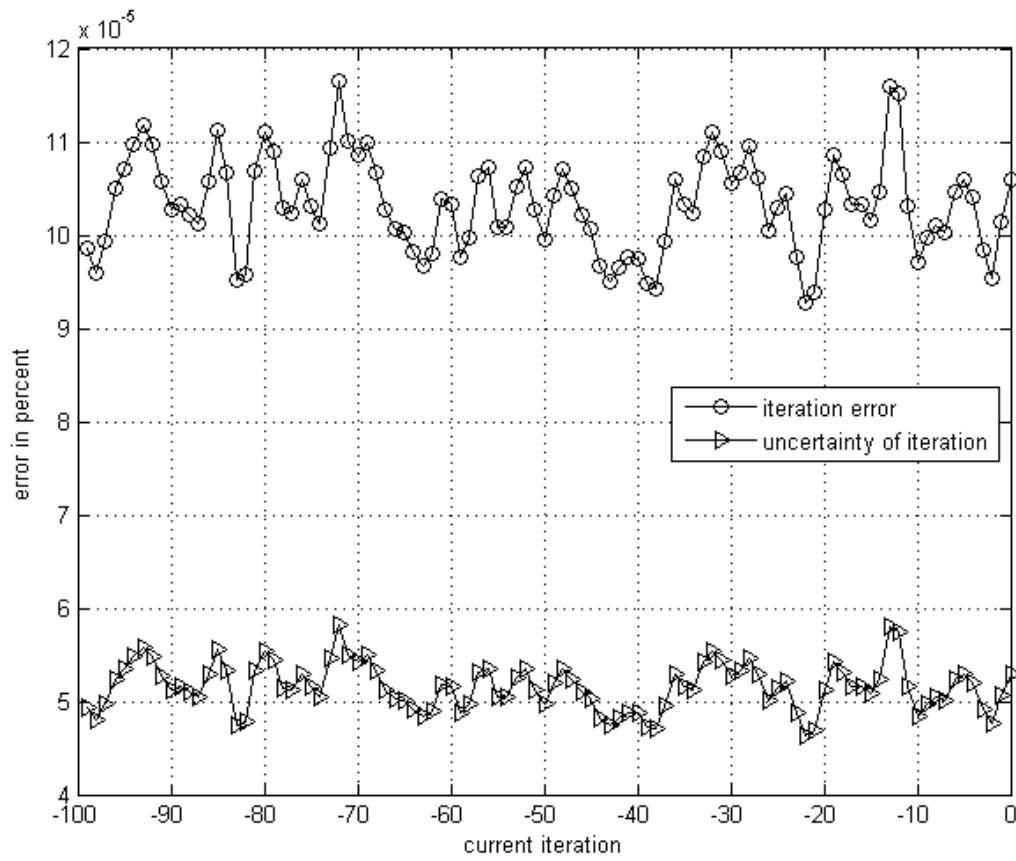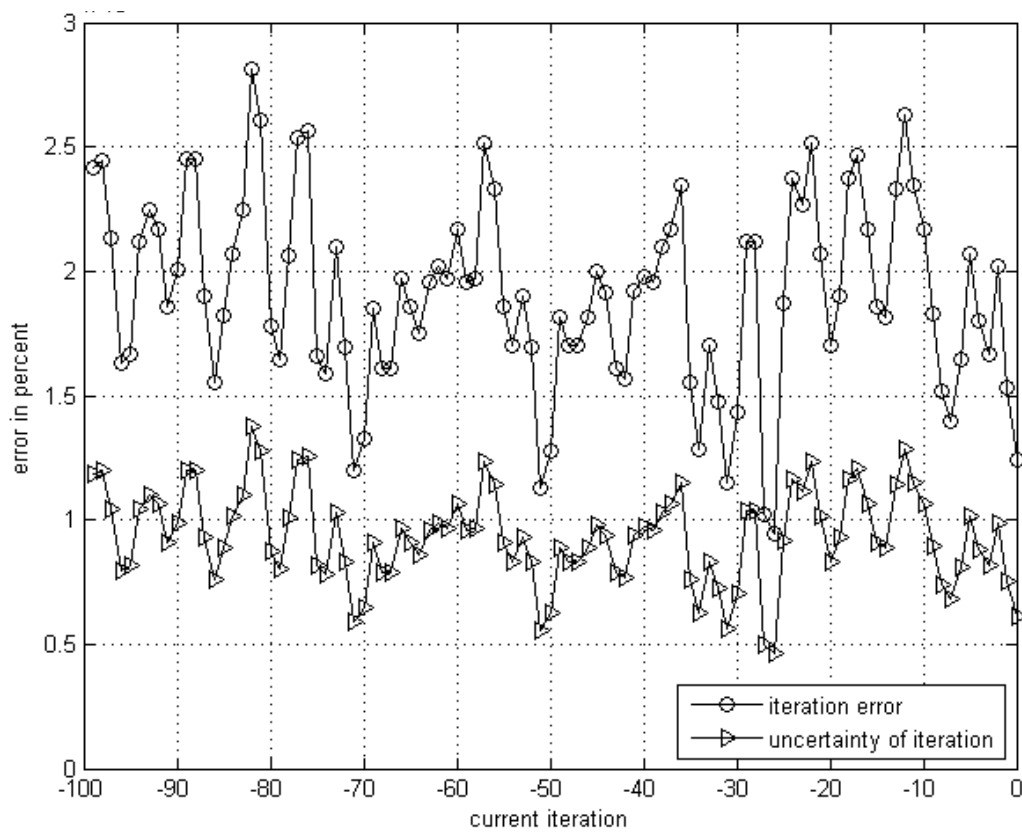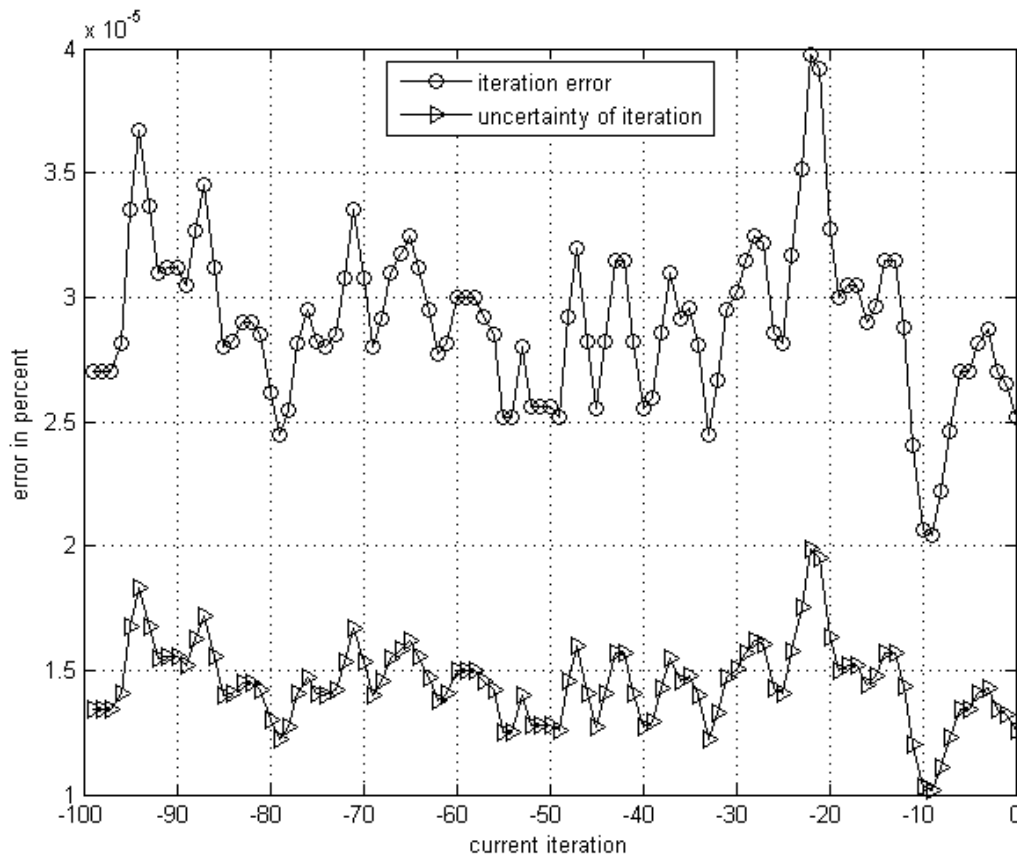
Figure 30

Figure 31

Figure 32

As can be seen in all graphs, the order of magnitude for both the iteration error and the uncertainty in iteration convergence is of 10^{-5}. Hence, the solution has converged. The residuals in Fluent never dropped below the predefined value of 10^{-4} which suggests that a relatively good initial guess has been found.